



Cite this: *Chem. Soc. Rev.*, 2017, 46, 6170

O–O bond formation in ruthenium-catalyzed water oxidation: single-site nucleophilic attack vs. O–O radical coupling

David W. Shaffer,  Yan Xie  and Javier J. Concepcion *

In this review we discuss at the mechanistic level the different steps involved in water oxidation catalysis with ruthenium-based molecular catalysts. We have chosen to focus on ruthenium-based catalysts to provide a more coherent discussion and because of the availability of detailed mechanistic studies for these systems but many of the aspects presented in this review are applicable to other systems as well. The water oxidation cycle has been divided in four major steps: water oxidative activation, O–O bond formation, oxidative activation of peroxide intermediates, and O₂ evolution. A significant portion of the review is dedicated to the O–O bond formation step as the key step in water oxidation catalysis. The two main pathways to accomplish this step, single-site water nucleophilic attack and O–O radical coupling, are discussed in detail and compared in terms of their potential use in photoelectrochemical cells for solar fuels generation.

Received 24th July 2017

DOI: 10.1039/c7cs00542c

rsc.li/chem-soc-rev

1. Introduction

The development of artificial photosynthesis (AP) is of paramount importance for a sustainable energy future that satisfies the growing worldwide energy demands while alleviating global climate change and preserving our ecosystems.^{1–7} As a result of its importance, the topic has been extensively reviewed,^{4,5,8–15} and a variety of systems and device architectures investigated.^{2,3,6,10,14,16–24} Catalytic approaches for fuel and oxidant formation vary from semiconductors and metal-oxides^{5,12,20,23} to more bio-inspired molecules and assemblies.^{3,4,11,15,18,25–28} One of the many challenges in realizing a useable device is developing catalysts that are efficient, stable, and active under conditions that are also favourable for the other parts of the device.²⁹

Water oxidation catalysis (WOC) is at the heart of this challenge as the ideal source of electrons and protons required for the conversion of solar energy into energy stored in chemical bonds. WOC has been identified as a rate-limiting bottleneck in AP,^{4,30} and acid-stable catalysis is a key area for potential impact in AP-relevant electrocatalysis and photoelectrocatalysis.^{16,29,31} Water oxidation is an energetically demanding and mechanistically complicated reaction that requires the loss of 4H⁺ and 4e[−] with the formation of an O–O double bond.

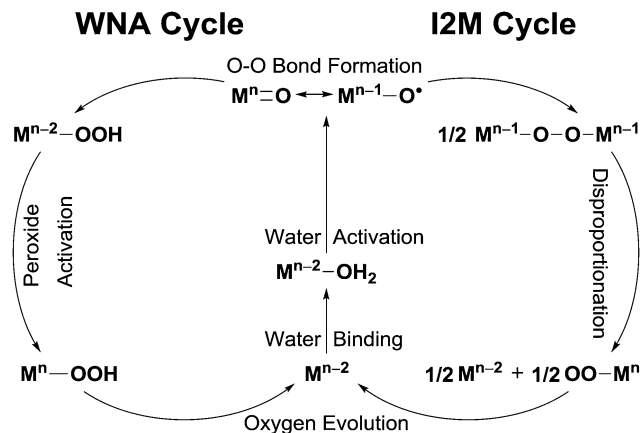
In nature, water oxidation takes place in the oxygen evolving complex (OEC) in photosystem II (PSII).^{32–40} The OEC is a Mn₄Ca cluster in close proximity to a tyrosine–histidine pair,

which mediates the oxidation of the OEC by oxidized chlorophyll *a* (P680⁺) through a series of proton-coupled electron transfer (PCET) steps. The Mn₄Ca cluster acts as a reservoir for the four oxidizing equivalents required for WOC, and redox levelling enabled by PCET results in the four single-electron oxidations of the OEC being within *ca.* 130 mV of one another.^{27,41} PCET is made possible by the drastic decrease in p*K*_a of Mn-bound water and hydroxide upon oxidation.^{27,42}

Two general types of mechanisms have been proposed for the initial formation of the O–O bond in water oxidation by the OEC. In one mechanism this key step involves an O–O radical coupling interaction of two metallo–oxyl radicals (I2M), with different variants existing regarding which two radicals are involved in the coupling.^{38,43–45} The second type of mechanism involves water nucleophilic attack (WNA) by a water molecule on an electrophilic Mn^V–oxo or Mn^{IV}–oxyl, with different variants proposed regarding whether this water molecule is free⁴⁶ or Ca-bound.^{47–50}

Related mechanisms for O–O bond formation are known for artificial molecular catalysts. These are shown in Scheme 1 and discussed in detail in the following section. Intramolecular O–O coupling through interaction of two metal–oxos (i-I2M) has been proposed for dinuclear Ru catalysts^{51–59} and intermolecular (or bimolecular) O–O coupling (I2M) has been reported for [Ru(bda)(L)₂], (bda is 2,2′-bipyridine-6,6′-dicarboxylate; L is a monodentate ligand).^{60–63} O–O bond formation in the latter system also takes place *via* radical coupling of two Ru^V–oxo moieties with significant Ru^{IV}–oxyl character, but in this case this key step is bimolecular.⁶¹ After many years of considering that two metal sites

Chemistry Division, Brookhaven National Laboratory, Upton, NY 11973-5000, USA.
 E-mail: jconcepc@bnl.gov



Scheme 1 Overview of water nucleophilic attack (WNA) and oxo-oxo coupling (I2M) mechanisms for water oxidation catalysis.

are required for WOC, the first well-defined molecular water oxidation catalyst, $[(\text{H}_2\text{O})\text{Ru}(\text{bpy})_2(\mu\text{-O})\text{Ru}(\text{bpy})_2(\text{OH}_2)]^{4+}$ (the blue dimer),⁶⁴ is now believed to follow a WNA mechanism.^{65–68} The WNA pathway is generally believed to be operative for most mononuclear catalysts, including $[\text{Ru}(\text{tpy})(\text{bpy})(\text{OH}_2)]^{2+}$ and its derivatives.^{69–71}

Many reviews are available in the literature covering water oxidation catalysis with molecular catalysts in a comprehensive way,^{72–86} including some focused on ruthenium-based catalysts,^{87–93} on surface-bound catalysts,^{94,95} on comparing different chemical oxidants,⁹⁶ and on differentiating homogeneous and heterogeneous catalysis.⁹⁷

In this review we focus on detailed mechanistic understanding of ruthenium-based molecular water oxidation catalysts and how this understanding can be used to design improved catalysts. We address here the four major stages of the water oxidation catalytic cycle outlined in Scheme 1, including (1) oxidative water activation, (2) O–O bond formation, (3) oxidative activation of peroxide intermediates, and (4) oxygen evolution. For each stage, we identify different catalytic pathways, provide prototypical catalyst examples, and consider strategies to accelerate catalysis. Our main focus is the key O–O bond formation step: What are the known mechanisms for this step? How are they optimized? What are their advantages and disadvantages? What fraction of the catalytic activity of a homogeneous catalyst is retained on the “heterogenized” version on an electrode surface? What types of catalysts are better suited for incorporation into solar cell devices?

2. Water oxidation mechanisms

In this review, catalysts will be classified based on how the O–O bond is formed.^{68,76,98} From this perspective, there are two major classifications of water oxidation catalysts: (1) those for which the O–O bond is formed between an electrophilic metal-oxo and a nucleophilic water molecule (WNA), and (2) those for which the O–O bond is formed between two M–O units with radical character (I2M). Discussed in detail below, it is important

to make a clear distinction between the mechanistic classification (WNA, I2M), the nuclearity of the catalyst (mononuclear, dinuclear, multinuclear), the number of active metal sites (single-site, two-site), and the molecularity of the mechanism with respect to catalyst (unimolecular, bimolecular). This section briefly reviews the two mechanisms, shown in Table 2, and key terminology, listed in Table 1.

2.1. Nuclearity, active sites, and molecularity

Catalysts are often categorized by their nuclearity, the number of metal centres per catalyst molecule. Mononuclear catalysts have a single metal centre, dinuclear catalysts have two, and multinuclear catalysts, such as structural OEC mimics,⁸³ have several. A catalyst can follow either of the aforementioned WOC mechanisms, regardless of the number of metal centres per molecule. This is illustrated by the examples in Table 2.

A related, but distinct, classification for catalysts is the number of metal centres that actively participate in catalysis, active sites. Active participation can be considered to be direct involvement in key activation and bond-formation steps, not including secondary interactions as a proton or electron relay. Catalysis does not necessarily involve active participation by all of the metal centres in a molecule. On the other hand, it may require multiple active metal centres from independent molecules. The term single-site catalysis indicates that the catalytic cycle can be completed with the participation of a single metal centre, though the term is sometimes unsuitably (in our opinion) used to mean mononuclear, which is often but not necessarily applicable. The only widely accepted mechanism for single-site water oxidation is the nucleophilic attack by a water molecule at an electrophilic metal-oxo (WNA), thus these two terms (single-site and WNA) are essentially interchangeable in this context. Single-site intramolecular O–O coupling from a bis-hydroxo or bis-oxo is possible, but to the best of our knowledge there is only one experimental example.⁹⁹ A precise counterpart to single-site is two-site. This is not a commonly used term in WOC because there is only one established two-site mechanism, which is more specifically referred to as the radical O–O coupling interaction of two metal-oxos (I2M). Table 2 illustrates the O–O bond forming step in each of these mechanisms for both mononuclear and dinuclear catalysts and provides examples of each.

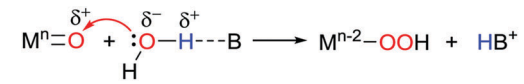
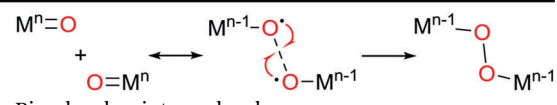
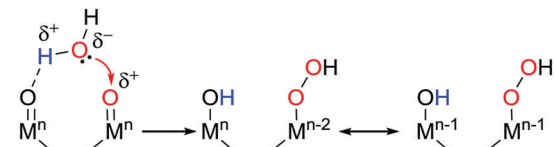
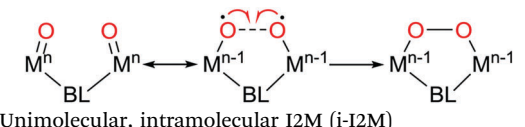
Finally, the molecularity is defined by the number of catalyst molecules required to complete the catalytic cycle. Though catalytic cycles contain many different reaction steps, it is most useful to differentiate them based on the overall molecularity with respect to the catalyst. The single-site WNA mechanism is typically unimolecular with respect to the catalyst. Also unimolecular are dinuclear two-site catalysts that utilize both of their metal sites in an intramolecular I2M cycle (i-I2M). A more commonly seen term is bimolecular, which strictly denotes a step involving two molecules, and in the context of WOC indicates that the catalytic cycle requires an intermolecular interaction between two catalyst molecules. A mononuclear or dinuclear catalyst requiring the coupling of two independent catalyst molecules is bimolecular. Table 2 indicates

Table 1 Terms and definitions relevant to water oxidation mechanisms

Mononuclear catalyst	Catalyst molecule with a single metal centre
Dinuclear catalyst	Catalyst molecule with two metal centres
Single-site catalysis	Catalysis in which all steps occur at a single metal centre
Two-site catalysis ^a	Catalysis which requires participation of two metal sites, contained in a single catalyst molecule or in separate catalyst molecules
Unimolecular catalysis ^a	Catalysis with no steps involving more than a single catalyst molecule
Bimolecular catalysis	Catalysis that includes a bimolecular step between two independent catalyst molecules
Atom-proton transfer (APT)	Transfer of a heavy atom, such as O, with concerted proton transfer to a base
Intramolecular atom-proton transfer (i-APT)	APT in which the heavy atom donor and proton acceptor are parts of the same molecule
Water nucleophilic attack (WNA)	Nucleophilic attack by a water molecule on an electrophilic metal-oxo, forming an O-O bond <i>via</i> APT
Interaction of two metal-oxos (I2M)	O-O bond formation between two metal-oxos, typically with radical character
Intramolecular interaction of two metal oxos (i-I2M)	I2M where the two metal-oxos are contained in a single catalyst molecule
Proton-coupled electron transfer (PCET)	An oxidation or reduction that coincides with loss or gain, respectively, of a proton
Intramolecular proton-coupled electron transfer (i-PCET)	PCET in which the proton donor and acceptor are parts of the same molecule

^a Two-site catalysis and unimolecular catalysis are not commonly used in regards to water oxidation catalysis, but are presented here as more precise counterparts to single-site catalysis and bimolecular catalysis, respectively.

Table 2 Representative O-O bond formation steps for water oxidation *via* water nucleophilic attack (WNA) and interaction of two metal-oxos (I2M) for mononuclear and dinuclear catalysts, including for each case the molecularity with respect to catalyst and examples. BL represents a bridging ligand, L is a pyridine-like ligand. See Charts 1-3 for structures

Catalyst nuclearity	Mechanism	
	Water nucleophilic attack (WNA, single-site)	Interaction of two metal-oxos (I2M, two-site)
Mononuclear	 <p>Unimolecular, base-mediated atom-proton transfer (APT) examples: [Ru^V(tpy)(bpz)(O)]³⁺ (5), [Ru^V(bpa)(L)₂(O)]⁻ (9)</p>	 <p>Bimolecular, intermolecular examples: [Ru^V(bda)(L)₂(O)]⁺ (8), <i>trans</i>-{[Ru^{IV}(tpym)(O)]₂(μ-bpp)}³⁺ (13)</p>
Dinuclear	 <p>Unimolecular, intramolecular atom-proton transfer (i-APT) example: [(O)(bpy)₂Ru^V(μ-O)Ru(bpy)₂(O)]⁴⁺ (blue dimer)</p>	 <p>Unimolecular, intramolecular I2M (i-I2M) examples: [Ru^{II}₂(O)₂(3,6-Bu₂Q)₂(btpyan)] (11), {[Ru^{IV}(tpy)(O)]₂(μ-bpp)}³⁺ (12)</p>

the molecularity of the various mechanistic possibilities relevant to WOC.

2.2. Mechanistic understanding driving catalyst design

A general consensus existed for many years in the water oxidation literature that two or more catalytic sites are required to make the O-O bond.^{100,101} As a result, many catalytic systems have been designed to bring two metal centres into close proximity in order to promote intramolecular O-O coupling.^{51,57,64,102-107} In recent years, evidence for the expected i-I2M mechanism has

validated this approach in several of these systems.^{53,55,56,59,108}

On the other hand, the mechanism of water oxidation by the blue dimer, first reported in 1982,⁶⁴ was debated well into the 2000s.^{65,66,109} The current interpretation that it goes through a WNA pathway was partly informed by work on mononuclear catalysts.^{65,66,110}

After receiving relatively little attention in the 1980s and 1990s,^{111,112} a mechanistic understanding of mononuclear ruthenium water oxidation catalysts began to develop in earnest in the late 2000s. Thummel and co-workers reported water

oxidation catalysis by mononuclear ruthenium catalysts but their initial reports did not establish whether these catalysts were pre-catalysts to multinuclear species that then followed intramolecular catalysis, were bimolecular catalysts, or acted as single-site catalysts.^{102,113} A first-order catalyst dependence was established in 2008, leading to the proposal of a single-site mechanism invoking a water nucleophilic attack on a $\text{Ru}^{\text{VI}}=\text{O}^{4+}$ intermediate.¹¹⁴ Nevertheless, the proposed mechanism involved two very high energy and likely unreachable species: $[\text{Ru}^{\text{IV}}(\text{py})_6]^{4+}$ and $[\text{Ru}^{\text{VI}}(\text{py})_6(\text{O})]^{4+}$ (py_6 represents six coordination sites occupied by pyridine-like ligands). Concurrently, Meyer and co-workers demonstrated a new single-site WNA mechanism,⁶⁹ which was further developed in a number of follow-up studies.^{87,115–117} The key aspect of the mechanism is O–O bond formation *via* concerted oxygen atom proton transfer (APT) from a $\text{Ru}^{\text{V}}=\text{O}$ intermediate to an incoming water molecule with concerted proton loss to an external base.^{70,92,118} This nomenclature originates from the analogy of this reaction to previously studied oxygen-atom transfer reactions from $\text{Ru}^{\text{IV}}=\text{oxo}$ to phosphines,^{119–122} and dimethylsulfide and dimethylsulfoxide,¹²³ and it is the equivalent of the WNA pathway proposed for the OEC. Understanding the APT step has allowed for new catalysts to be developed that facilitate the O–O bond forming step by incorporating a proton acceptor into the secondary coordination sphere, enabling intramolecular APT (i-APT).^{124–127}

A short time later, additional mononuclear ruthenium-based catalysts were reported by the groups of Sakai and Sun, both of which proposed new WOC mechanisms. Sakai showed first-order catalyst dependence for mononuclear ruthenium–polypyridyl complexes,^{128,129} and later proposed O–O bond formation *via* radical coupling between a ruthenium–oxyl and a cerium–hydroxyl.^{130,131} A new family of catalysts incorporating anionic ligands was developed by Sun.⁶⁰ These remarkably fast catalysts were the first mononuclear catalysts shown to use the I2M mechanism to form O_2 , and the family remains among the best water oxidation catalysts known to date.^{61,132} The transition state (TS) interactions in the oxo–oxo coupling step have been probed theoretically and experimentally, leading to further optimized catalysts.^{132–135}

2.3. The single-site WNA mechanism

Single-site O–O bond formation has been proposed for mononuclear,^{71,79,136,137} multinuclear,^{64,66,67} and nanoparticle^{138,139} catalysts. The key step involves the attack of a water molecule on an electron-deficient metal–oxo species, with simultaneous proton transfer to a hydrogen-bonded proton acceptor, to generate a hydroperoxide intermediate.^{69,70,114} The left side of Table 2 shows the O–O bond-forming step for representative mononuclear and dinuclear catalysts. There are many potential proton acceptors, such as a water molecule,^{116,117} the basic form of a buffer,^{70,94} strategically positioned bases,^{124,127} or another metal–oxo group.^{52,64,66,67} At high pH, the concentration of hydroxide is sufficient for it to act as the nucleophile without an additional base, making the term WNA a bit of a misnomer under these conditions.

Catalytic rates for single-site catalysts can be limited either by an oxidation step,¹²⁴ by the O–O bond forming step, or by the O_2 release step.^{70,116} Each step in the cycle has a first-order dependence on catalyst, and the oxidation steps are also first-order in oxidant. These catalysts tend to be slower than I2M catalysts. This is in part due to the higher potentials required to produce a sufficiently electrophilic metal–oxo. The O–O bond forming step can be accelerated by increasing the basicity or effective concentration of the proton acceptor (the pH need not necessarily change).⁷⁰ Any PCET oxidation steps can be similarly accelerated.

2.4. The two-site I2M mechanism

As opposed to the electrophilic metal–oxos that favour the WNA mechanism, the I2M mechanism is favoured by more electron-rich catalysts that have more oxyl radical character in their activated state. These catalysts have more electron density around the ruthenium centre, which results in the population of orbitals with Ru–O antibonding character. Because of their reactive nature, the $\text{Ru}^{\text{n}}=\text{O}/\text{Ru}^{\text{n}-1}\text{O}^\bullet$ state of these catalysts are not easily characterized, and the contribution of the oxyl radical configuration is typically invoked based on DFT calculations.^{52,55,59,61,63,140} Experimental evidence of ruthenium(IV)–oxyl character has been reported for other systems.^{141–143} When the O–O bond is formed by the coupling of two metal–oxyl radicals, a peroxo bridge between the two metal centres is formed. As shown on the right side of Table 2, this process can occur intramolecularly (i-I2M) in multinuclear complexes,^{52,53,58} a cluster,¹⁴⁴ or a nanoparticle,¹⁴⁵ or intermolecularly (bimolecular I2M) between two independent molecules.^{60,61,132,146}

The rate-determining step in these systems may be an oxidation step, the oxo–oxo coupling step, or the O_2 release step.^{61,98} Because bimolecular steps are more sensitive to catalyst concentration, catalysts requiring an intermolecular coupling step will be rate-limited by that step at low enough catalyst concentration.⁹⁸ This step can be accelerated by increasing favorable secondary interactions between molecules, with particular attention to the expected TS geometry.^{132,135,147} Thermodynamic stabilization can only go so far; any organized TS between two molecules will have a significant entropic penalty.¹³⁵ This is avoided by including the two metal centres in a single dinuclear catalyst, with the trade-offs being additional synthetic challenges and additional constraints on the active site geometry.^{52,58} The latter may be alleviated by more flexible assemblies.^{105,148}

2.5. Other mechanisms

There are a couple of other WOC mechanisms that have been proposed, but are not discussed in detail here because they are not widely applicable to many catalysts or conditions.

A catalyst with two oxo or hydroxo groups in a *cis* arrangement may be able to undergo intramolecular O–O coupling at a single site. To the best of our knowledge, there are just two accounts of this. The first is an experimental study by Milstein and co-workers where O–O bond formation occurs in a $[(\text{L})\text{Ru}(\text{OH})_2]$ pincer complex, ultimately generating 0.5 equivalents of O_2 .⁹⁹ Isotopic labelling studies with ^{18}O support the intramolecular

nature of the O–O bond formation step, which was proposed to release H₂O₂. Nevertheless, in this study the O–O bond formation is initiated by irradiation and the involvement of hydroxyl radical cannot be ruled out. The second example is a theoretical study by Baik and co-workers on a *cis*-Mn^V(O)₂ complex, which was proposed to generate an η²-O₂ *via* a high-spin intermediate.¹⁴⁹ This mechanism has not yet been well-established and the only experimental example is believed to proceed through disproportionation of H₂O₂.

An alternative radical O–O coupling mechanism has been proposed by Sakai and coworkers, in which the coupling occurs between Ru^V=O and Ce^{IV}-OH.^{130,131} This mechanism is difficult to experimentally differentiate from the WNA mechanism because they obey the same rate law, which is first order in catalyst and first order in cerium(IV). In any case, it is not widely applicable as it could only be available under specific conditions with cerium(IV) as a sacrificial oxidant.

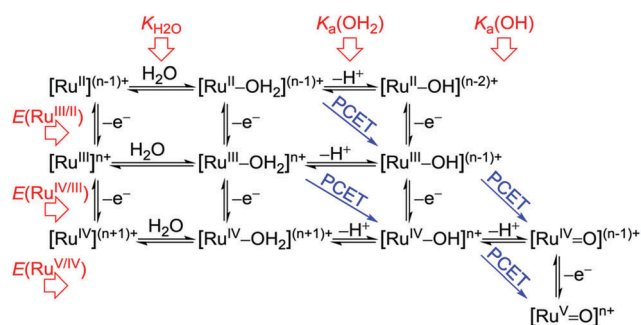
3. Water activation

The initial phase in any WOC mechanism requires the first water molecule to be oxidatively activated, resulting in a metal-oxo or metal-oxyl.¹⁵⁰ This typically involves several oxidative steps and the binding of water, if it is not already bound. PCET oxidations, involving protons from the water or from the catalyst molecule itself, serve to temper the oxidation potentials that would otherwise be demanding to reach a highly oxidized metal-oxo.¹⁵¹ A generic overview of the pathways for oxidative water activation is shown in Scheme 2.

Catalysts whose rate is limited by one of these steps will obey the rate law in eqn 1, which shows the first order dependence on both catalyst concentration and oxidant concentration. We will use rate constants of the general form $k_{x,y}$, where x is the reaction order with respect to catalyst and y is the reaction order with respect to oxidant, and assign an activity of 1 to water.

$$\text{rate} = k_{1,1}[\text{Ru}][\text{oxidant}] \quad (1)$$

Most ruthenium-based water oxidation catalysts are six-coordinate Ru^{II} complexes with a pseudo-octahedral geometry due to the high stability of the d⁶ electronic configuration for these complexes. There are two general cases based on the



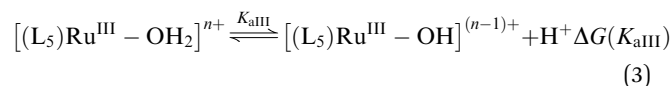
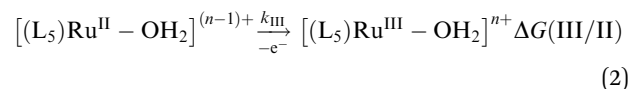
Scheme 2 Pathways for oxidative activation of water by ruthenium-based catalysts.

presence or absence of a water molecule as one of the ligands in the initial coordination environment.

3.1 Catalysts with pre-coordinated water

In the first case, five of the six coordination sites in the octahedron are occupied by ancillary ligands (often involving a number of pyridine rings) and the sixth coordination site is occupied by a water molecule, [(L₅)Ru^{II}(OH₂)]⁽ⁿ⁻¹⁾⁺.

3.1.1 Ru^{III/II} couple. The first step in the oxidative activation of the first water molecule is the oxidation of Ru^{II} to Ru^{III}. The rate constant for electron transfer from Ru^{II}-OH₂⁽ⁿ⁻¹⁾⁺, k_{III} in eqn (2), is typically very fast regardless of the electron acceptor (the anode in electrochemical experiments or a sacrificial oxidant in chemical or photochemical experiments). The resulting Ru^{III}-OH₂ⁿ⁺ species is a stronger acid than the original Ru^{II}-OH₂⁽ⁿ⁻¹⁾⁺ species by several pK_a units and it is in acid–base equilibrium with the corresponding Ru^{III}-OH⁽ⁿ⁻¹⁾⁺ species, eqn (3). The rate constants for the acid–base equilibrium depend on the nature and concentration of the proton acceptor. Whether the Ru^{III/II} couple is a PCET or stepwise process depends on the redox potential for the couple, K_{aIII} , and pH.



Typical examples of this case are [Ru^{II}(tpy)(bpy)(OH₂)]²⁺ (**1**, tpy is 2,2':6',2''-terpyridine; bpy is 2,2'-bipyridine)¹⁵² and [Ru^{II}(Mebimpy)(bpy)(OH₂)]²⁺ (**2**, Mebimpy is 2,6-bis(1-methylbenzimidazol-2-yl)pyridine),^{115,116,118} shown in Chart 1. For the sake of simplicity, we will use numerals to represent all oxidation states of the catalysts (*i.e.* the overall catalytic systems) and use formulae to describe specific species. Sakai and co-workers

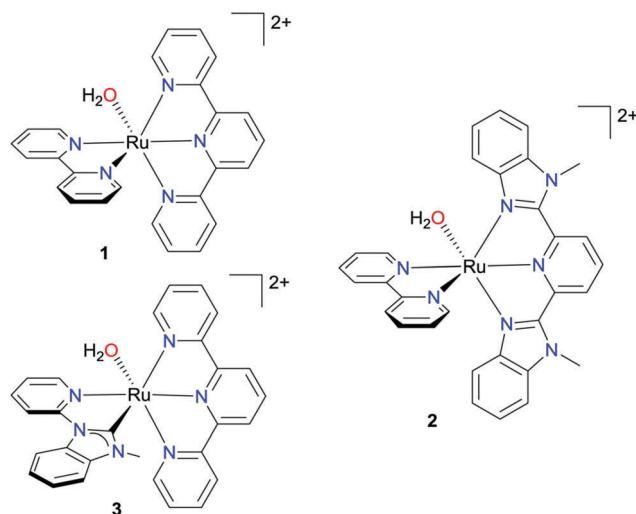


Chart 1 Chemical structures of [Ru^{II}(tpy)(bpy)(OH₂)]²⁺ (**1**), [Ru^{II}(Mebimpy)(bpy)(OH₂)]²⁺ (**2**), and [Ru^{II}(tpy)(Mebimpy)(OH₂)]²⁺ (**3**).

reported **1** as an active water oxidation catalyst in 2009.¹²⁸ Berlinguette *et al.* studied in detail the influence of electron-donating and electron-withdrawing groups on catalytic activity of analogues of **1**.^{153–155} Both **1** and **2** display reversible one-electron Ru^{III/II} couples, with $E_{1/2}$ values 1.06 V and 0.82 V, respectively, at pH 1.0 (all potentials discussed here are referenced to NHE unless otherwise specified).^{115,156,157} The Mebimpy ligand in **2** is more electron-rich and has higher energy π^* orbitals than tpy, allowing less $d\pi-\pi^*$ back bonding than in **1**. This results in a lower $E_{1/2}$ for the Ru^{III/II} couple for **2**, and a more stable Ru^{II} in **1**. The electron-rich ligand in **2** also affects the pK_a of the bound water molecule, stabilizing Ru^{III}-OH₂³⁺ with respect to Ru^{III}-OH²⁺: pK_{aIII} is 1.6 for **1** and 2.5 for **2**. Below pK_{aIII} , the couple is Ru^{II}-OH₂²⁺ to Ru^{III}-OH₂³⁺ (eqn (2)), and above it is a PCET oxidation Ru^{II}-OH₂²⁺ to Ru^{III}-OH²⁺ (eqn (2) + eqn (3)). Pourbaix diagrams plotting $E_{1/2}$ vs. pH are convenient for examining the relationship between oxidation potentials and pK_a values. The $1e^-/1H^+$ PCET nature of the Ru^{II}-OH₂²⁺/Ru^{III}-OH²⁺ couple at intermediate pH for **1** and **2** is indicated by a slope of approximately 59 mV pH⁻¹ above their pK_{aIII} in the Pourbaix diagrams in Fig. 1.

To control catalysis, it is desirable to have independent control over these two interconnected factors ($E_{1/2}(\text{Ru}^{\text{III/II}})$ and pK_{aIII}). The protonation state of the Ru^{III} form of the catalyst affects a number of aspects of the water activation steps, as discussed further in Section 3.1.2. The catalyst [Ru^{II}(tpy)(Mebim-py)(OH₂)²⁺ (**3**, Mebim-py is 3-methyl-1-pyridylbenzimidazol-2-ylidene, see Chart 1)^{118,158,159} is a good example of increasing pK_{aIII} without affecting $E_{1/2}(\text{Ru}^{\text{III/II}})$. As in **1**, the low-lying π^* orbitals in tpy stabilize Ru^{II} through $d\pi-\pi^*$ back bonding. The carbene ligand is also a good π -acceptor, but its strong σ -donation *trans* to the aqua ligand significantly stabilizes Ru^{III}-OH₂³⁺ with respect to Ru^{III}-OH²⁺. Illustrated in the Pourbaix diagram in Fig. 1, this results in an increase of pK_{aIII} from 1.6 for **1** to 5.5 for **3**, a difference of ~ 4 pK_a units, while the $E_{1/2}$ value for Ru^{III/II} at pH 1.0 remains similar at 1.11 V for **3** and 1.06 V for **1**. It is also

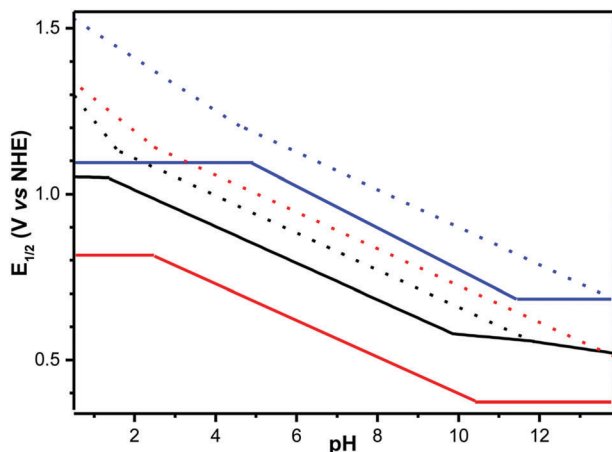
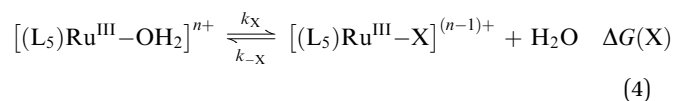


Fig. 1 Pourbaix diagrams showing the pH-dependent behaviour for the Ru^{III/II} (solid lines) and Ru^{IV/III} (dashed lines) couples for [Ru^{II}(tpy)(bpy)(OH₂)²⁺ (**1**, black), [Ru^{II}(Mebimpy)(bpy)(OH₂)²⁺ (**2**, red), and [Ru^{II}(tpy)(Mebim-py)(OH₂)²⁺ (**3**, blue).^{118,156}

important to note the steep divergence between the Ru^{III}-OH₂³⁺/Ru^{II}-OH₂²⁺ and Ru^{IV}=O²⁺/Ru^{III}-OH₂³⁺ potentials below pK_{aIII} . The $2H^+/1e^-$ nature of the latter couple causes $E_{1/2}$ to change by 120 mV per pH unit, and the higher Ru^{IV/III} potential contributes to a stronger driving force for oxidation, which is discussed further in Section 4.1.1. Thus, the ligand properties can be tuned to affect other aspects of catalysis without significantly changing the Ru^{III/II} potential.

Factors affecting the Ru^{III/II} potential and pK_{aIII} also play a role in promoting or counteracting deleterious anion substitution for water (anation) in Ru^{III}-OH₂. Shown in eqn (4), buffer anions can displace the neutral aqua ligand in ruthenium(III) complexes. This is particularly problematic in complexes with a stable Ru^{III}-OH₂³⁺: those with a high $E_{1/2}(\text{Ru}^{\text{III/II}})$ that are more electrophilic, and those with a high pK_{aIII} that disfavour Ru^{III}-OH²⁺. Anation is a reversible equilibrium, but it delays further catalysis and the reverse reaction can become rate-limiting. Such is the case for **1** and the blue dimer.⁶⁶ Though **3** has an even higher pK_{aIII} , the carbene's strong σ -donation increases the lability of the water/anion binding site, increasing the rate of the reverse reaction and offsetting the negative effects of anation.



In contrast to the strongly donating Mebim-py ligand in **3**, strongly withdrawing ligands are associated with a low pK_{aIII} and a high $E_{1/2}(\text{Ru}^{\text{III/II}})$. Though increasing the Ru^{III/II} potential seems counterproductive, it in fact provides an alternative path for oxidative activation that precludes anation. As discussed above, electron-withdrawing ligands with low-lying π^* orbitals effect a low pK_{aIII} , favouring the deprotonated Ru^{III}-OH²⁺ form over Ru^{III}-OH₂³⁺. While these catalysts have a higher Ru^{III/II} potential, the resulting Ru^{III}-OH²⁺ is more easily oxidized than Ru^{III}-OH₂³⁺ and sufficiently withdrawing ligands can lead to a situation where the Ru^{IV/III} oxidation is more facile than the Ru^{III/II}. For example, [Ru^{II}(tpy)(bpm)(OH₂)²⁺ (**4**, bpm is 2,2'-bipyrimidine) and [Ru^{II}(tpy)(bpz)(OH₂)²⁺ (**5**, bpz is 2,2'-bipyrazine), which are shown in Chart 2, both have pK_{aIII} values below 0, and Ru^{III}-OH²⁺ is the dominant form from pH 0 to 14.^{69,160} The result is that $E_{1/2}(\text{Ru}^{\text{IV/III}})$ is less positive than $E_{1/2}(\text{Ru}^{\text{III/II}})$ and disproportionation of Ru^{III}-OH²⁺ to Ru^{II}-OH₂²⁺ and Ru^{IV}=O²⁺ is

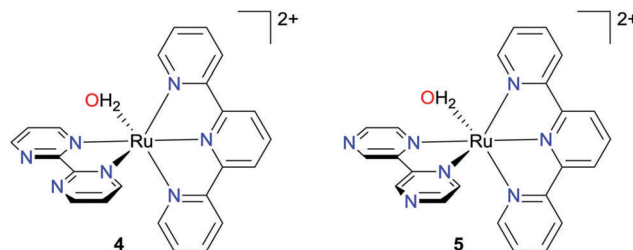


Chart 2 Chemical structures of [Ru^{II}(tpy)(bpm)(OH₂)²⁺ (**4**) and [Ru^{II}(tpy)(bpz)(OH₂)²⁺ (**5**).

spontaneous. The oxidation effectively becomes a $2\text{H}^+/2\text{e}^-$ process in the presence of an anodic potential or excess oxidant.

3.1.2. Ru^{IV/III} couple. The importance of the Ru^{III} to Ru^{IV} oxidative activation step has been overlooked in the literature. It is the rate-limiting step of the water oxidation cycle for many catalysts.¹⁶¹ However, because the following oxidative activation step from Ru^{IV} to Ru^V often takes place at a higher potential, this final step is often assigned as rate limiting. The Ru^{IV/III} couple is typically kinetically inhibited for several reasons, including its high potential, proton loss, and formation of a double bond to oxygen.^{161–163} Cyclic voltammograms for these complexes typically exhibit kinetically distorted waves for the Ru^{IV/III} couple.¹⁵⁷ This is in contrast to the oxidation of Ru^{IV}=O²⁺ to Ru^V=O³⁺, which involves very little reorganization and can be faster than the Ru^{IV/III} oxidation even in the presence of a high anodic potential or excess oxidant.

For catalysts 1–5, Ru^{IV}-OH³⁺ is very acidic and the final species in this oxidation is Ru^{IV}=O²⁺. Its formation involves the loss of one or two protons (depending on pH and pK_{aIII}) and the formation of a multiple bond between Ru and O. In the absence of PCET pathways, high energy intermediates such as Ru^{III}-(O⁻)⁺ or Ru^{IV}=(OH⁺)³⁺ are unavoidable.^{161,162} In addition, the formation of a Ru–O multiple bond requires significant reorganizational energy. These requirements lead to high kinetic barriers. Even when PCET pathways are available (with high buffer concentrations,¹⁶² activated electrodes)^{151,164} they require highly organized transition states with preformed hydrogen bonded intermediates, which introduces an entropic penalty.

Thermodynamically speaking, electronic factors that lead to higher values of pK_{aIII} also correspond to higher values of E_{1/2} for the Ru^{IV}=O²⁺/Ru^{III}-OH₂³⁺ couple at low pH. This is reflected in the Pourbaix diagram in Fig. 1, which shows a slope of 120 mV per pH unit for this process below pK_{aIII}, indicative of the 2H⁺/1e⁻ process. The value of E_{1/2}(Ru^{IV/III}) directly affects the Gibbs free energy change for the O–O bond formation step, ΔG(O–O), which is determined not only by the potential of the Ru^V=O³⁺/Ru^{IV}=O²⁺ couple, but actually by the average of the Ru^{IV}=O²⁺/Ru^{III}-OH₂³⁺ and the Ru^V=O³⁺/Ru^{IV}=O²⁺ couples, as discussed in Section 4.1.1.

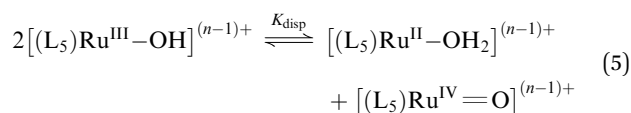
Another impediment to efficient Ru^{IV/III} oxidation is anation of electrophilic Ru^{III} centres,⁶⁶ which tend to have a higher affinity for anions than neutral ligands, as mentioned above and shown in eqn (4). For example, catalyst 1 has a pK_{aIII} of 1.6 and Ru^{III}-OH₂³⁺ dominates below pH 1.6. As a result, 1 is deactivated at low pH, undergoing complete anation in solution or surface-bound at pH 1.0 in 0.10 M HNO₃, HClO₄ and HOTf.

There are several strategies to avoid or outcompete deleterious anation. Maintaining a low pK_{aIII} by introducing electron-withdrawing ligands favours the Ru^{III}-OH²⁺ form, which is easily oxidized and resists substitution because it is already “anated”. This is a cause for the higher catalytic activity of 4 (TOF = 7.5 × 10⁻⁴ s⁻¹) and 5 (1.4 × 10⁻³ s⁻¹) with pK_{aIII} < 0, compared to 1 (1.9 × 10⁻⁴ s⁻¹) with pK_{aIII} = 1.6.¹¹⁸ Unfortunately, this strategy also pushes the Ru^{V/IV} couple to a more positive value, which leads to slower kinetics for this step and higher overpotentials.

A better approach is to make the water coordination site labile by manipulating the site in the *trans* position, as is the case for 3. Analogously to 1, 3 undergoes complete anation at pH 1, but the *trans* effect of the carbene makes the water-anion exchange process very fast, and further catalyst oxidation is not significantly affected by anation.¹¹⁸ The *trans* effect is manifested in the longer ruthenium-aqua distance in the crystal structure of 3 compared to 1. Additionally, the aqueous synthesis of 3 directly affords the aqua complex from the chloro, whereas 1 requires the use of silver salts or neat triflic acid for this exchange.¹¹⁸ The *trans* effect might also accelerate the oxygen evolution step although this claim cannot be made for 3 because this step is not usually rate limiting.

Another strategy to avoid anation is to make Ru^{III}-OH₂³⁺ electron-rich, affecting the relative affinities for anions and H₂O. For more electron-rich 2, Ru^{III}-OH₂³⁺ is favoured at low pH over Ru^{III}-X²⁺ and further oxidation to Ru^{IV}=O²⁺ is not limited by anation of Ru^{III}-OH₂³⁺. As a result, 2 outperforms 1 in terms of TOFs, overpotentials, TONs, and faradaic efficiency for O₂ generation.^{118,165}

In addition to direct chemical or electrochemical oxidation, disproportionation of Ru^{III}-OH²⁺ or Ru^{III}-OH₂³⁺, as mentioned above and shown in eqn (5), provides an alternative pathway to reach Ru^{IV}=O²⁺.^{157,166} This is another reason for the much higher catalytic activity of 4 and 5 compared to 1, with disproportionation constants K_{disp}(5) > K_{disp}(4) ≫ K_{disp}(1) = 6.7 × 10⁻⁷ M⁻¹ s⁻¹.¹⁶⁶ The value of K_{disp} reflects the proximity of the Ru^{IV/III} and Ru^{III/II} potentials in 4 and 5. The large and positive separations between the Ru^{IV/III} and the Ru^{III/II} potentials in 2 and 3 (ΔE = +470 mV¹¹⁵ and +380 mV,¹⁵⁹ respectively, at pH 1.0) are consistent with small values of K_{disp}. Access to Ru^{IV}=O²⁺ from Ru^{III}-OH₂³⁺ for these catalysts is limited by direct chemical or electrochemical oxidation, which is very slow and likely to be rate limiting for these two catalysts, with E_{1/2} values of 1.29 V and 1.49 V at pH 1.0 for 2 and 3, respectively.



3.1.3. Ru^{V/IV} couple. The oxidation to Ru^V=O is the last oxidative activation step and it leads to the active form of the catalysts.^{69,116} For complexes 1–5 the transition from Ru^{IV}=O is a pH-independent, pure outer sphere one-electron transfer with relatively small reorganizational energy. As such, it is often faster than the preceding oxidation step, despite taking place at a higher potential. For many catalysts with a rate-limiting oxidation step in the catalytic cycle, the oxidation of Ru^{IV}=O⁽ⁿ⁻¹⁾⁺ to Ru^V=Oⁿ⁺ is often assigned as the rate-determining step when, more often than not, the preceding oxidation to Ru^{IV} is actually slower.

3.2. Catalysts without pre-coordinated water

In the second class of catalysts, all six coordination sites are initially occupied by ancillary ligands, with no water molecule in the coordination environment, [(L₆)Ru^{II}]⁽ⁿ⁻¹⁾⁺.

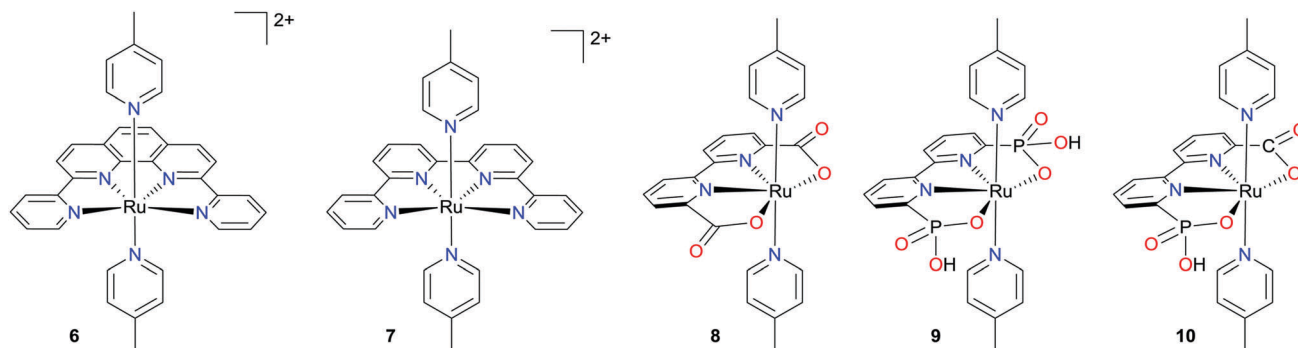
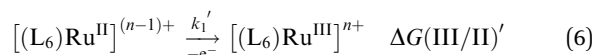


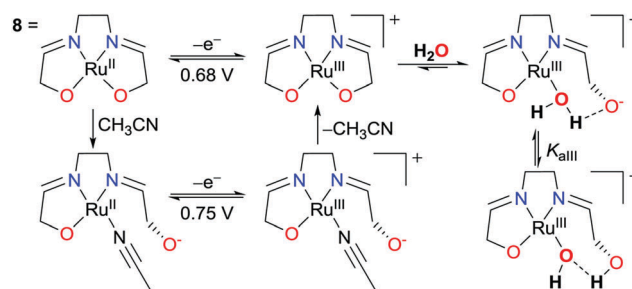
Chart 3 Chemical structures of catalysts without pre-coordinated water, $[\text{Ru}(\text{dpp})(\text{pic})_2]^{2+}$ (**6**), $[\text{Ru}(\text{qtpy})(\text{pic})_2]^{2+}$ (**7**), $[\text{Ru}(\text{bda})(\text{pic})_2]$ (**8**), $[\text{Ru}(\text{bpaH}_2)(\text{pic})_2]$ (**9**) and $[\text{Ru}(\text{bpHc})(\text{pic})_2]$ (**10**).

3.2.1. Ru^{III/II} couple. Because it is associated with minimal reorganization, these complexes typically exhibit a fast, pH-independent, one-electron Ru^{III/II} oxidation, shown in eqn (6), although more complex situations may arise because of equilibration of $[(\text{L}_6)\text{Ru}^{\text{II}}]^{(n-1)+}$ with $[(\text{L}_5)\text{Ru}^{\text{II}}\text{-OH}_2]^{(n-1)+}$ or $[(\text{L}_6)\text{Ru}^{\text{II}}]^{n+}$ with $[(\text{L}_5)\text{Ru}^{\text{III}}\text{-OH}_2]^{n+}$. For the cases discussed in more detail in this review, the electron-rich, anionic nature of the equatorial ligands lower oxidation potentials and avoid anation. Alternatively, one might consider these catalysts pre-anated because the rate and favourability of water coordination to the various oxidation states of the catalysts is an additional consideration in these systems, which in turn affects the rates and potentials for the following oxidations.



Shown in Chart 3, there are now many examples of this type of catalyst in the literature, such as $[\text{Ru}(\text{dpp})(\text{pic})_2]^{2+}$ (**6**),^{113,114,167,168} $[\text{Ru}(\text{qtpy})(\text{pic})_2]^{2+}$ (**7**),¹⁶⁹ $[\text{Ru}(\text{bda})(\text{pic})_2]$ (**8**),^{60,61} $[\text{Ru}(\text{bpaH}_2)(\text{pic})_2]$ (**9**)^{124,125} and $[\text{Ru}(\text{bpHc})(\text{pic})_2]$ ¹²⁶ (**10**, dpp is 2,9-di(pyridin-2-yl)-1,10-phenanthroline; qtpy is 2,2':6',2'':6'',2'''-quaterpyridine; bda²⁻ is 2,2'-bipyridine-6,6'-dicarboxylate; bpa²⁻ is 2,2'-bipyridine-6,6'-bis(hydrogenphosphonate); bpHc²⁻ is 2,2'-bipyridine-6-hydrogenphosphonate-6'-carboxylate; pic is 4-picoline). Analogues of catalysts **8**, **9**, and **10** where 4-picoline is replaced by isoquinoline (isq) will be denoted as **8'**,⁶¹ **9'**,¹²⁴ and **10'**,¹²⁶ respectively. For this review we will focus on catalysts **8–10**, in addition to **1–5**, because their corresponding water oxidation mechanisms are the most understood and they are more closely related.

While catalysts **8–10** have generally low oxidation potentials by virtue of their electron-rich ligands, their coordinative saturation and potentially labile ligand 'arms' lead to more complex oxidative pathways. Catalyst **8** undergoes fast reversible oxidation to Ru^{III}, which binds a water molecule as a labile carboxylate group de-coordinates, shown in Scheme 3.¹⁷⁰ Complex **8** displays a one-electron reversible couple at 0.68 V in pH 1.0 aqueous solution corresponding to oxidation of $[(\kappa^4\text{-bda})\text{Ru}^{\text{II}}(\text{pic})_2]$ to $[(\kappa^4\text{-bda})\text{Ru}^{\text{III}}(\text{pic})_2]^+$. Water soluble versions of **8** exist in aqueous solution as $[(\kappa^4\text{-bda})\text{Ru}^{\text{II}}(\text{pic})_2]$ based on ¹H-NMR,¹⁷⁰ but when CH₃CN is added, the dominant form becomes $[(\kappa^3\text{-bda})\text{Ru}^{\text{II}}(\text{pic})_2(\text{CH}_3\text{CN})]$.^{134,171} In the latter, one of



Scheme 3 Oxidations and solvent coordination behaviour associated with the Ru^{III/II} couple of $[\text{Ru}(\text{bda})(\text{pic})_2]$ (**8**), showing only the immediate equatorial ligand environment.

the carboxylate arms is de-coordinated and replaced by a CH₃CN molecule. With added CH₃CN, the equivalent Ru^{III/II} couple appears at 0.75 V and corresponds to oxidation of $[(\kappa^3\text{-bda})\text{Ru}^{\text{II}}(\text{pic})_2(\text{CH}_3\text{CN})]$ to $[(\kappa^3\text{-bda})\text{Ru}^{\text{III}}(\text{pic})_2(\text{CH}_3\text{CN})]^+$.¹⁷¹ These equilibria are illustrated in Scheme 3.

It has been proposed recently that coordination expansion takes place with water binding at six-coordinate $[(\kappa^4\text{-bda})\text{Ru}^{\text{III}}(\text{pic})_2]^+$ to yield 19-electron, seven-coordinate $[(\kappa^4\text{-bda})\text{Ru}^{\text{III}}(\text{pic})_2(\text{OH}_2)]^+$.¹⁷² This proposal is based on the existence of two different forms of Ru^{III} in aqueous solution from EPR studies, with one of the forms having lower symmetry. These results can also be explained without invoking unlikely 19-electron Ru complexes: based on DFT calculations $[(\kappa^3\text{-bda})\text{Ru}^{\text{III}}(\text{pic})_2(\text{OH}_2)]^+$ is the dominant form of this complex in aqueous solution, although close in energy to $[(\kappa^4\text{-bda})\text{Ru}^{\text{III}}(\text{pic})_2]^+$.^{126,170} Furthermore, $[(\kappa^3\text{-bda})\text{Ru}^{\text{III}}(\text{pic})_2(\text{OH}_2)]^+$ is in acid-base equilibrium with $[(\kappa^3\text{-bdaH})\text{Ru}^{\text{III}}(\text{pic})_2(\text{OH})]^+$ ($K_{\text{aIII}} = 1.07$) where one of the protons of the water molecule has been transferred to the open carboxylate group, as shown in Scheme 3.¹²⁶ This will allow for fast PCET oxidation to seven-coordinate $[(\kappa^4\text{-bda})\text{Ru}^{\text{IV}}(\text{pic})_2(\text{OH})]^+$, as discussed below. The existence of six coordinate $[(\kappa^4\text{-bda})\text{Ru}^{\text{III}}(\text{pic})_2]^+$ (higher symmetry) and six coordinate $[(\kappa^3\text{-bda})\text{Ru}^{\text{III}}(\text{pic})_2(\text{OH}_2)]^+$ and $[(\kappa^3\text{-bdaH})\text{Ru}^{\text{III}}(\text{pic})_2(\text{OH})]^+$ (lower symmetry) in aqueous solution can also account for the EPR results reported by Sun and co-workers¹⁷² without invoking 19-electron Ru species.

The behaviour of complex **9**, which has phosphonic acid groups in place of the carboxylic acids of **8**, is quite different.¹²⁴

It also displays a one-electron reversible couple at 0.68 V in pH 1.0 but it is pH-dependent due to the increased acidity of the phosphonic acid protons, which are lost upon oxidation from Ru^{II} to Ru^{III}. This couple corresponds to oxidation of $[(\kappa^4\text{-bpaH}_2)\text{Ru}^{\text{II}}(\text{pic})_2]$ to $[(\kappa^4\text{-bpa})\text{Ru}^{\text{III}}(\text{pic})_2]^-$. The Ru–O bonds in $[(\kappa^4\text{-bpa})\text{Ru}^{\text{III}}(\text{pic})_2]^-$ ¹²⁴ are stronger than in $[(\kappa^4\text{-bda})\text{Ru}^{\text{III}}(\text{pic})_2]^+$,¹⁷⁰ which is manifested in shorter Ru–O bond distances, and the O–Ru–O angle is significantly smaller (112.1° vs. 126.4°), imposing a steric impediment for water coordination. As a result, $[(\kappa^4\text{-bpa})\text{Ru}^{\text{III}}(\text{pic})_2]^-$ is the dominant form in solution and the following oxidative activation step is a pure outer sphere, pH-independent electron transfer step, requiring a much higher potential, as discussed below.

Complex **10**¹²⁶ is a hybrid catalyst designed by combining features of complexes **8** and **9**. It also displays a one-electron reversible couple at 0.65 V in pH 1.0 that is pH-dependent because of the phosphonic acid proton in the bpa-like side. But because of the presence of a carboxylate group on the other side, similar behaviour to **8** occurs: $[(\kappa^4\text{-bpc})\text{Ru}^{\text{III}}(\text{pic})_2]$ binds water in aqueous solution to form $[(\kappa^3\text{-bpc})\text{Ru}^{\text{III}}(\text{pic})_2(\text{OH}_2)]$, which is in acid–base equilibrium with $[(\kappa^3\text{-bpcH})\text{Ru}^{\text{III}}(\text{pic})_2(\text{OH})]$ where one of the protons of the water molecule has been transferred to the open carboxylate arm ($K_{\text{aIII}} = 0.15$). As explained in the following section, water coordination at Ru^{III} introduces a pH-dependence on the following oxidative activation step that results in decreased overpotentials for water oxidation and significantly faster oxidative activation steps for complex **10** compared to complex **9**.

3.2.2. Ru^{IV/III} couple. The Ru^{IV/III} couple for catalysts **8–10** results in coordination expansion to 7-coordinate, 18-electron Ru^{IV}–OH species. These hydroxide complexes, which are much less acidic than those for catalysts **1–5**, are the most stable Ru^{IV} form. Their formation, as opposed to Ru^V=O, does not involve multiple-bond formation between Ru and O and requires lower reorganizational energy.

In the case of **8**, oxidation of $[(\kappa^3\text{-bdaH})\text{Ru}^{\text{III}}(\text{pic})_2(\text{OH})]^+$ is facile with $E_{1/2} = 1.10$ V at pH 1.0 to generate seven-coordinate $[(\kappa^4\text{-bda})\text{Ru}^{\text{IV}}(\text{pic})_2(\text{OH})]^+$. Water coordination at the Ru^{III} state, allowed by the labile carboxylate group, introduces a pH-dependence on the Ru^{IV/III} couple and avoids charge build-up. The value of the acid–base equilibrium constant ($K_{\text{aIII}} = 1.07$) between $[(\kappa^3\text{-bda})\text{Ru}^{\text{III}}(\text{pic})_2(\text{OH}_2)]^+$ and $[(\kappa^3\text{-bdaH})\text{Ru}^{\text{III}}(\text{pic})_2(\text{OH})]^+$ indicates a low barrier for the proton transfer between the two forms.^{126,170} The fast equilibrium allows the more facile oxidation of $[(\kappa^3\text{-bdaH})\text{Ru}^{\text{III}}(\text{pic})_2(\text{OH})]^+$ to $[(\kappa^3\text{-bdaH})\text{Ru}^{\text{IV}}(\text{pic})_2(\text{OH})]^{2+}$ to dominate, which is followed by (or in concert with) proton loss to the buffer and re-coordination of the carboxylate to generate a stable 18-electron $[(\kappa^4\text{-bda})\text{Ru}^{\text{IV}}(\text{pic})_2(\text{OH})]^+$. This complex is the most highly oxidized intermediate in these systems to be isolated and characterized.⁶⁰ The combination of the PCET nature of the oxidation, electron density donation to the Ru center from the dianionic ligand, and lower-order Ru–O bond, results in faster oxidative activation steps over a narrower potential window compared to catalysts **1–5**.

The Ru^{IV/III} couple for catalyst **9** is pH-independent over a large pH range and precedes water binding.¹²⁴ Because the

most stable Ru^{III} form of the complex is $[(\kappa^4\text{-bpa})\text{Ru}^{\text{III}}(\text{pic})_2]^-$, potential levelling by proton loss is not available, explaining the high Ru^{IV/III} couple measured at 1.57 V at pH 1.0. This oxidative activation step is slow compared to that of complex **8**, both chemically and electrochemically. Water coordination follows, proceeding through coordination expansion from 16-electron $[(\kappa^4\text{-bpa})\text{Ru}^{\text{IV}}(\text{pic})_2]$ to 18-electron $[(\kappa^4\text{-bpa})\text{Ru}^{\text{IV}}(\text{pic})_2(\text{OH})]^-$, coincident with proton transfer to the bulk.

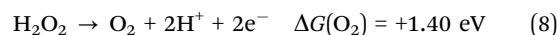
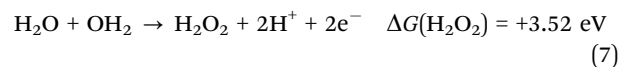
Hybrid complex **10** incorporates the best features of complexes **8** and **9**.¹²⁶ As in the case of **8**, the labile carboxylate side enables water coordination at the Ru^{III} state, and oxidation to Ru^{IV} via PCET avoids charge build-up and reduces redox potentials. The multifunctional phosphonate side provides additional charge compensation, and also acts as a pendant base in later steps, allowing access to fast intramolecular PCET (i-PCET) (discussed below). The most stable Ru^{III} complex, $[(\kappa^3\text{-bpc})\text{Ru}^{\text{III}}(\text{pic})_2(\text{OH}_2)]$, undergoes PCET oxidation to $[(\kappa^4\text{-bpc})\text{Ru}^{\text{IV}}(\text{pic})_2(\text{OH})]$, measured at 1.4 V at pH 1.0.

3.2.3. Ru^{V/IV} couple. As in the case of catalysts **1–5**, the oxidation to Ru^V=O is the last oxidative activation step and it leads to the active form of the catalysts.^{61,124,126} However, catalysts **8–10** display significantly lower Ru^{V/IV} potentials than **1–5**. One reason is the anionic character of the bda²⁻, bpa⁴⁻, and bpc³⁻ ligands that increases the electron density on the Ru centre and compensates the overall charge. Another reason is the seven-coordinate nature of Ru^V=O for catalysts **8–10**, making them relatively much more electron-rich than other Ru^V-oxos. Last, but not least, the Ru^{IV}–OH/Ru^V=O couple is pH-dependent, and charge accumulation is avoided by release of a proton.

In addition, for catalysts **9** and **10**, the pendant phosphonate can act as the initial proton-acceptor through intramolecular PCET (i-PCET), before releasing the proton to the bulk solution, circumventing the need for a precisely positioned external base in the TS and thusly reducing kinetic barriers for oxidative activation. For example, as $[(\kappa^4\text{-bpc})\text{Ru}^{\text{IV}}(\text{pic})_2(\text{OH})]$ is oxidized, fast intramolecular proton transfer from the hydroxide to the uncoordinated phosphonate provides $[(\kappa^4\text{-bpHc})\text{Ru}^{\text{V}}(\text{pic})_2(\text{O})]^+$, which is followed by slower proton loss to the buffer to finally form $[(\kappa^4\text{-bpc})\text{Ru}^{\text{V}}(\text{pic})_2(\text{O})]$. The i-PCET pathway is also operative in several following oxidation steps and is pivotal in accelerating the overall rate for these single-site catalysts, further discussed below.

4. O–O bond formation

Water oxidation can be separated into two major 2-electron stages: O–O bond formation and O₂ evolution. For thermodynamic purposes, these two steps are similar to the oxidation of water to hydrogen peroxide and further oxidation of hydrogen peroxide to release O₂, eqn (7) and (8).



A total of 4.92 eV ($4\text{e}^- \times 1.23$ V) of free energy is required for water oxidation. Between these two steps, ~71% of the energy

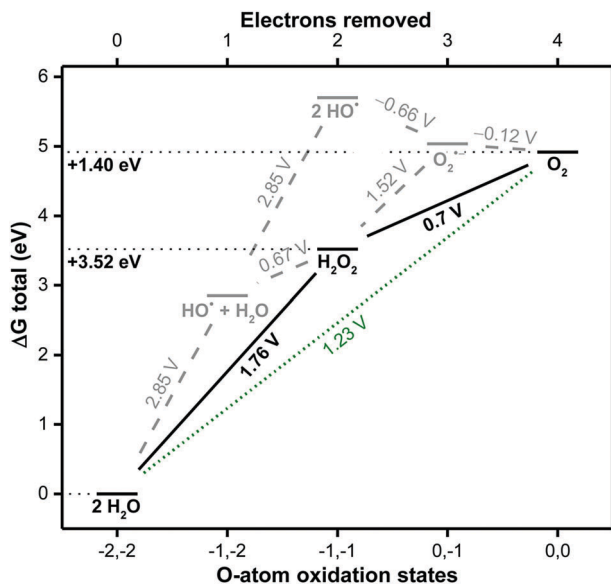
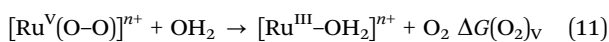
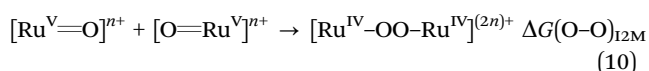
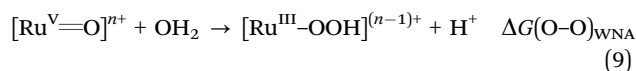


Fig. 2 Latimer–Frost diagram showing pathways and intermediates for the oxidation of water to oxygen.

is associated with the formation of the O–O bond, making this the key step. The 3.52 eV associated with peroxide formation corresponds to two electrons at 1.76 V, which is 0.53 V greater than the overall 4-electron thermodynamic potential of 1.23 V per electron. Once the O–O bond is formed, just 1.40 eV more (0.70 V per electron) reaches the total free energy required. A visual representation is provided by the Latimer–Frost diagram for oxygen, which is shown in Fig. 2. As can be seen by the slopes, a sequence avoiding H_2O_2 and involving single-electron intermediates such as HO^\bullet is even less efficient. In other words, regardless of the pathway, the steps leading up to O–O bond formation make up the most energetically demanding part of the overall reaction. It could be said as well that the oxidation state change from -2 to -1 for each O atom is more difficult than the following -1 to 0 oxidation.

Analogous steps exist for water oxidation in natural and artificial photosynthesis. The O–O bond formation step leads to a hydroperoxide or peroxide intermediate, eqn (9) or eqn (10), related to H_2O_2 in eqn (7).^{53,55,61,69,115,116} Oxygen evolution from a peroxide intermediate, eqn (11), is analogous to the O_2 evolution step in eqn (8) (further discussed in Section 5). While the thermodynamics of these steps are obviously not the same as the uncatalyzed reactions, it is reasonable to expect the trend to be the same: the most thermodynamically demanding portion of water oxidation is O–O bond formation.



A catalytic system has the advantage of being able to operate in smaller steps involving electrons and protons while avoiding

high-energy intermediates. For water oxidation to occur, several oxidative activation steps are required, both preceding and following the key O–O bond formation step. The two water molecules in eqn (7) must be activated in order to be reactive toward one another for O–O bond formation. This is achieved by simultaneously removing electrons and protons from one of the water molecules to reach a more reactive species. The $1\text{e}^-/1\text{H}^+$ oxidation of water to generate a hydroxyl radical requires a high energy price, but this can be avoided by coordinating the water molecule to a transition metal catalyst. As shown in the previous section, ruthenium catalysts can provide low-energy PCET pathways to generate a reactive $\text{Ru}=\text{O}$, which is primed to form an O–O bond with either a water molecule or another catalyst molecule.

4.1. Single-site WNA catalysts

An activated $\text{Ru}^{\text{V}}=\text{O}$ is typically quite electron-poor, making it a good electrophile. Shown in eqn (9), the second water molecule can now act as a nucleophile and attack the electron-deficient $\text{Ru}^{\text{V}}=\text{O}^{n+}$ to form the O–O bond. Unfortunately, water is not a good nucleophile and the reaction shown in eqn (9) is slow. Deprotonation of the second water molecule generates the hydroxide ion, which is a powerful nucleophile that can quickly react with $\text{Ru}^{\text{V}}=\text{O}^{n+}$ without requiring simultaneous proton loss. However, the pK_a of water is 15.7 and significant concentrations of hydroxide ion only exist at high pH. Therefore, efficient pathways must be developed that take into account the need for a proton loss over the full pH range.

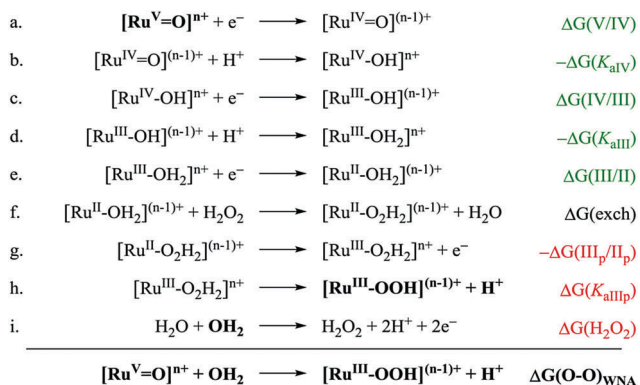
The rate of this step is proportional to the concentration of catalyst, as shown in eqn (12). The presence of a base as the proton acceptor introduces a second term in the rate law, shown in eqn (13), which typically dominates when it is more basic than water.^{70,171} Of course, these rate laws will only be observed if this step limits the rate of catalysis.

$$\text{rate} = k_{1,0}[\text{Ru}] \quad (12)$$

$$\text{rate} = k_{1,0}[\text{Ru}] + k_{1,0,\text{B}}[\text{Ru}][\text{base}] \quad (13)$$

Scheme 1 shows an overview of the water nucleophilic attack mechanism for water oxidation with a single-site catalyst. Catalysts 1–5, 9 and 10 follow this mechanism, with small variations for each family. The product of the O–O bond-forming step, as shown in eqn (9), is the corresponding $\text{Ru}^{\text{III}}-\text{OOH}^{(n-1)+}$, which must then be further oxidized in order to release oxygen as discussed below.

4.1.1 Thermodynamic analysis. A thermodynamic analysis reveals important aspects that need to be accounted for to achieve the key O–O bond-forming step in ruthenium-catalyzed water oxidation. Listed in Scheme 4, the goal of this thermochemical cycle is to provide a framework for understanding the many factors that affect $\Delta G(\text{O-O})_{\text{WNA}}$ and to guide the design of new catalysts capable of more favourable O–O bond formation, not to afford an exact value. This is done by assembling a list of simple reactions which sum to the reaction in eqn (9), and for which ΔG can be measured or estimated based on electrochemical or spectroscopic measurements. These include eqn (7)



Scheme 4 Thermodynamic analysis for O–O bond formation between an activated $\text{Ru}^{\text{V}}=\text{O}^{n+}$ catalyst molecule and a water molecule. Green indicates favourable contributions and red indicates unfavourable ones.

and a simple stepwise pathway of electron transfers, proton transfers, and ligand exchange, between $\text{Ru}^{\text{V}}=\text{O}^{n+}$ and $\text{Ru}^{\text{III}}\text{-OOH}^{(n-1)+}$. These thermochemical cycles do not imply the participation of any particular intermediates, but they can reveal contributors to the overall driving force for the O–O bond-forming step.

Constructing this thermochemical cycle requires a series of simple reactions between $\text{Ru}^{\text{V}}=\text{O}^{n+}$ and $\text{Ru}^{\text{III}}\text{-OOH}^{(n-1)+}$. The first steps are the reverse of the oxidative activation steps discussed above, and can be measured experimentally: $\Delta G(\text{V/IV})$, $-\Delta G(K_{\text{aIV}})$, $\Delta G(\text{IV/III})$, $-\Delta G(K_{\text{aIII}})$, and $\Delta G(\text{III/II})$ (steps a–e). These steps can lead to $\text{Ru}^{\text{II}}\text{-OH}_2$, which can exchange the aqua ligand for a bound hydrogen peroxide molecule (step f). It is necessary to include the Ru^{II} state because the energy of the $\text{H}_2\text{O}/\text{H}_2\text{O}_2$ exchange, $\Delta G(\text{exch})$, can be reasonably estimated, while exchange at Ru^{III} is less likely to occur for most catalysts. Oxidation, $\Delta G(\text{III}_p/\text{II}_p)$ (step g), and deprotonation, $\Delta G(K_{\text{aIIIp}})$ (step h), results in the product, $\text{Ru}^{\text{III}}\text{-OOH}^{(n-1)+}$. These quantities are not as easily measured, but can be estimated based on the corresponding hydroxide complexes and typical differences between H_2O and H_2O_2 . Finally, the 2-electron oxidation of water to H_2O_2 , eqn (7) (step i), balances the remaining species. In this scheme, the electron- and proton-transfer steps are separated, but these can be considered as a single ΔG value for the PCET couple when it is available.

The greatest thermodynamic aspect to consider in Scheme 4 is the staggering value of $\Delta G(\text{H}_2\text{O}_2) = +3.52$ eV, corresponding to eqn (7) (step i). The extent to which the other contributors to the thermochemical cycle can offset this quantity is indicative of how effective a catalyst is. $\Delta G(\text{V/IV})$ and $\Delta G(\text{IV/III})$ (steps a and c) are the main favourable contributors. Therefore, for a good catalyst, the $\text{Ru}^{\text{V/IV}}$ and $\text{Ru}^{\text{IV/III}}$ couples should be high enough to mediate catalysis, but close to each other to reduce the overall overpotential required to reach the former. In the best case scenario, $\Delta G(\text{V/IV}) = \Delta G(\text{IV/III})$. This is often overlooked in the literature. Often only the $\text{Ru}^{\text{V/IV}}$ couple is considered when estimating driving forces for O–O bond formation.

A subtle, but significant result, is the favourable contribution of $-\Delta G(K_{\text{aIV}})$ associated with the protonation of $\text{Ru}^{\text{IV}}=\text{O}^{(n-1)+}$

to generate $\text{Ru}^{\text{IV}}\text{-OH}^{n+}$ (step b). For catalysts 1–5 $\text{p}K_{\text{aIV}}$ values are below 0, while for catalysts 9 and 10 they are higher than 6. This translates to a free energy contribution in favour of O–O bond formation of more than 0.36 eV for 9 and 10 compared to 1–5!

The overall significance of the steps involving the Ru^{III} and Ru^{II} states depend on the difference in $E_{1/2}$ and $\text{p}K_{\text{a}}$ between the aqua complexes (steps d and e) and hydrogen peroxide complexes (steps g and h), and the energy of exchange between them (step f). A favourable but unexpected contributor is $\Delta G(\text{III/II})$, but it is significantly counterbalanced by $-\Delta G(\text{III}_p/\text{II}_p)$. It is fairly safe to assume that $\Delta G(\text{III/II})$ is slightly greater than $\Delta G(\text{III}_p/\text{II}_p)$ for most systems. The difference in $\text{p}K_{\text{a}}$ values between $\text{Ru}^{\text{III}}\text{-O}_2\text{H}_2^{n+}$ and $\text{Ru}^{\text{III}}\text{-OH}_2^{n+}$ can be estimated based on the difference in $\text{p}K_{\text{a}}$ values between H_2O (15.7) and H_2O_2 (11.7). It can be assumed that $\text{p}K_{\text{aIIIp}} \approx \text{p}K_{\text{aIII}} - 4$ and the sum of $-\Delta G(K_{\text{aIII}})$ and $\Delta G(K_{\text{aIIIp}})$ in Scheme 4 is $0.059(\text{p}K_{\text{aIIIp}} - \text{p}K_{\text{aIII}}) = -0.24$ eV. This difference in $\text{p}K_{\text{a}}$ values contributes about 0.24 eV of free energy in favour of O–O bond formation. The free energy for exchange between H_2O and H_2O_2 , $\Delta G(\text{exch})$, could potentially be determined spectrophotometrically by measuring the corresponding equilibrium constant. Unfortunately, attempts to do so for catalysts 1, 2, 4, and 5 were unsuccessful because these complexes catalyze very efficiently the disproportionation of H_2O_2 into O_2 and H_2O . In any case, this value is anticipated to be small and have a minor contribution.

Breaking down the O–O bond-forming step into simple steps with readily measureable or estimable energies has provided guidelines for catalyst design, regardless of whether the component steps involve actual intermediates or not. As an example, available data for 2 leads to $\Delta G(\text{O-O})_{\text{WNA}} \approx -0.06$ eV (-1.4 kcal mol $^{-1}$), assuming $\Delta G(\text{exch}) = 0$.¹¹⁵ This analysis shows that catalyst design should be prioritized to (1) store enough energy through the $\text{Ru}^{\text{V/IV}}$ and $\text{Ru}^{\text{IV/III}}$ oxidations to drive the reaction, while minimizing the difference between them, (2) maximize the $\text{p}K_{\text{aIV}}$ of $\text{Ru}^{\text{IV}}\text{-OH}$, and lastly (3) increase the $\text{Ru}^{\text{III/II}}$ potential. These factors represent the ability of the catalyst to mitigate the inherent difficulty in O–O bond formation.

4.1.2. Base-assisted O–O bond formation. As previously mentioned, an important aspect in the O–O bond formation step in eqn (9) is the requirement for the loss of a proton from the water molecule acting as the nucleophile. Thermodynamically, the $\text{p}K_{\text{a}}$ of the conjugate acid of the proton acceptor affects the free energy change for this process, and it is more favourable with bases stronger than the water discussed above. Kinetically, the details of how this proton transfer takes place (*e.g.*, concerted *vs.* stepwise) are fundamental to lowering the activation barrier for this step.

For catalysts 1–5 at pH 1.0, bulk water acts as the proton acceptor, with proton transfer from the incoming water molecule occurring in concert with formal O-atom transfer from the $\text{Ru}^{\text{V}}=\text{O}$ (APT). Considering $\text{p}K_{\text{a}}(\text{H}_3\text{O}^+) = -1.7$, H_2O is a poor proton acceptor. Not surprisingly, these catalysts are very slow under these conditions, although slow O–O bond formation is not the only reason for their poor performance, as discussed in previous sections. For catalyst 2, the replacement of H_2O by H_2PO_4^- ($\text{p}K_{\text{a}} = 2.15$), CH_3COO^- ($\text{p}K_{\text{a}} = 4.75$), HPO_4^{2-} ($\text{p}K_{\text{a}} = 7.2$),

and PO_4^{3-} ($\text{p}K_{\text{a}} = 12.32$) as the proton acceptor was shown to enhance water oxidation rates spanning 4 orders of magnitude.⁷⁰ Nevertheless, the need for a highly organized TS in the O–O bond formation step involving three different species imposes a significant entropic penalty to the free energy of activation.

4.1.3. Intramolecular atom proton transfer (i-APT). Insight into solving this entropy problem can be gained from the first synthetic molecular water oxidation catalyst, $[(\text{H}_2\text{O})\text{Ru}(\text{bpy})_2-(\mu\text{-O})\text{Ru}(\text{bpy})_2(\text{OH}_2)]^{4+}$, the blue dimer.⁶⁴ In this catalyst, as the incoming water performs nucleophilic attack on one of the two $\text{Ru}^{\text{V}}=\text{O}$ moieties, a proton of the water molecule is transferred to the adjacent $\text{Ru}^{\text{V}}=\text{O}$ group.^{65,66} This intramolecular atom-proton transfer (i-APT) process decreases the entropic penalty on the free energy of activation for O–O bond formation because the proton acceptor is part of the catalyst, and it is pre-positioned in the appropriate orientation. Even so, $\text{Ru}^{\text{V}}=\text{O}$ is a poor proton acceptor and this reflects negatively on the enthalpy of activation in this system.

Multifunctional diphosphonate bipyridine ligands address both the entropic and enthalpic kinetic requirements for O–O bond formation.¹²⁴ In complex **9**, the phosphonate ligand is pre-positioned to establish a strong hydrogen-bonding interaction with one of the protons of the incoming water molecule. In addition, the phosphonate group is a good proton acceptor ($\text{p}K_{\text{a}} \approx 1$) and this contributes to a more favourable enthalpy of activation in the O–O bond formation process. The overall result is a very low calculated free energy of activation $\Delta G^{\ddagger}(\text{calc.}) = +10.2 \text{ kcal mol}^{-1}$ for O–O bond formation for **9** *via* i-APT. For complex **8**, $\Delta G^{\ddagger}(\text{calc.})$ is $+29.8 \text{ kcal mol}^{-1}$ following the APT pathway with H_2O as the proton acceptor.¹²⁴ This is part of the reason that it favours the bimolecular radical pathway. The main contribution to $\Delta G^{\ddagger}(\text{calc.})$ for APT in **8** comes from the entropic term with $-T\Delta S^{\ddagger} = +20.6 \text{ kcal mol}^{-1}$ compared to $+11.3 \text{ kcal mol}^{-1}$ for **9**. In addition, H_2O is a poor proton acceptor and it results in a higher ΔH^{\ddagger} for **8** ($+9.3 \text{ kcal mol}^{-1}$, calculated) than for **9** ($-1.1 \text{ kcal mol}^{-1}$, calculated), with phosphonate as the proton acceptor *via* i-APT for the latter.

Careful design of both the first and second coordination spheres in **9** leads to kinetically fast O–O bond formation, but is this process thermodynamically more favourable than for **1–5** or **8**? Multifunctionality of the bpa ligand is important in providing charge compensation and redox potential levelling with loss of protons. In fact, all species involved in the catalytic

cycle for **9** are negatively charged. As a result, the $\text{Ru}^{\text{V/IV}}$ ($E_{1/2} = 1.46 \text{ V}$, calculated) and $\text{Ru}^{\text{IV/III}}$ ($E_{1/2} = 1.57 \text{ V}$ exp., 1.41 V calc.) couples overlap, which is close to the ideal condition. In addition, $\text{p}K_{\text{aIV}} = 8.1$ contributes more than 0.48 eV in free energy in favour of O–O bond formation compared to **1–5**. Despite the additional charge compensation, pendant base activity, and fast O–O coupling in **9**, catalysis is ironically limited by a pH-independent, high potential $\text{Ru}^{\text{IV/III}}$ couple that precedes water coordination and further activation.

Hybrid complex **10** shares the fast O–O bond formation *via* i-APT, while overcoming the disadvantage of unfavourable oxidation.¹²⁶ As discussed above, water coordination at Ru^{III} instead of Ru^{IV} , through decoordination of the carboxylate side of bpc^{3-} , allows the $\text{Ru}^{\text{IV/III}}$ couple to be proton coupled, decreasing its potential by 200 mV relative to **9**. In fact, each oxidation step in the catalytic cycle of **10** is proton-coupled. The onset of water oxidation catalysis for **10** is also 200 mV lower compared to **9**. The i-APT O–O bond-forming pathway is analogous to **9**, with a calculated barrier of $+11.7 \text{ kcal mol}^{-1}$. Though the lower oxidation potentials equate to less driving force from $\Delta G(\text{V/IV})$ and $\Delta G(\text{IV/III})$, the overall rate is accelerated because O–O bond formation is not rate-limiting. This is an example of the successful optimization of one step (O–O bond formation) creating the need to optimize another step (oxidative activation) to accelerate overall catalysis.

10 reaches TOFs of 60 s^{-1} for cerium(IV)-driven water oxidation, two orders of magnitude faster than **9** and three times faster than **8** under the same conditions. The homologue of **10** with isoquinoline in place of 4-picoline, $[\text{Ru}(\text{bpHc})(\text{isq})_2]$, **10'**, reaches TOFs over 100 s^{-1} . These rates are comparable to those of the OEC on a per site basis, more than two orders of magnitude faster than **9'** and almost two times faster than the bda^{2-} analogue, **8'**. For **10'** $\Delta G^{\ddagger}(\text{calc.})$ is $+9.8 \text{ kcal mol}^{-1}$ for O–O bond formation *via* i-APT with $-T\Delta S^{\ddagger} = +12.0 \text{ kcal mol}^{-1}$ and $\Delta H^{\ddagger} = -2.2 \text{ kcal mol}^{-1}$. Kinetic parameters for selected catalysts are included in Table 3.

4.2. Radical O–O coupling

An alternative way to make the key O–O bond is the radical coupling of two $\text{Ru}=\text{O}$ moieties with significant radical oxyl character, as shown in eqn (10). Catalysts that follow this pathway can operate at lower potentials because, unlike the WNA pathway, they do not require a very electrophilic $\text{Ru}=\text{O}$.

Table 3 Kinetic parameters for water oxidation catalyzed by coordinatively-saturated ruthenium catalysts

Catalyst	$k_{1,1}^a$ ($\text{M}^{-1} \text{ s}^{-1}$)	$k_{2,0}^b$ ($\text{M}^{-1} \text{ s}^{-1}$)	TOF _{max} (s^{-1})	TON _{max}	Ref.
$[(\text{bda})\text{Ru}(\text{pic})_2]$ (8)	1.8×10^4	5.3×10^5	32	2000	61 and 98
$[(\text{bda})\text{Ru}(\text{isq})_2]$ (8')	6.7×10^4	1.8×10^7	780	11 300	61, 98 and 133
$[(\text{bda})\text{Ru}(6\text{-F-isq})_2]$	7.1×10^4	1.9×10^7	1000	24 000	133 and 135
$[(\text{bda})\text{Ru}(6\text{-OMe-isq})_2]$	1.3×10^5	1.2×10^8	1274	14 860	135
$[(\text{bda})\text{Ru}(6,7\text{-OMe})_2\text{-isq})_2]$	1.7×10^5	3.4×10^8	1034	7215	135
$[(\text{bpaH}_2)\text{Ru}(\text{pic})_2]$ (9)	1.6×10^3	n/a	0.82	—	124
$[(\text{bpaH}_2)\text{Ru}(\text{isq})_2]$ (9')	1.9×10^3	n/a	0.97	—	124
$[(\text{bpHc})\text{Ru}(\text{pic})_2][\text{ClO}_4]$ (10)	1.2×10^5	n/a	58	—	126
$[(\text{bpHc})\text{Ru}(\text{isq})_2]$ (10')	1.6×10^5	n/a	107	1600	126

^a Rate = $k_{1,1}[\text{catalyst}][\text{Ce}^{\text{IV}}]$ for a rate-limiting oxidation step (eqn (1)). ^b Rate = $k_{2,0}[\text{catalyst}]^2$ for a rate-limiting bimolecular coupling step (eqn (14)).

The two Ru=O moieties can be part of a binuclear (or multinuclear) catalyst (i-I2M)^{52,53,55} or originate from two separate molecules (I2M).^{61,63} The former intramolecular step is unimolecular in catalyst and obeys the rate law in eqn (12), while the latter intermolecular step is bimolecular in catalyst and obeys the rate law in eqn (14). The experimentally observed rate law depends on which step is limiting the overall catalytic rate under the particular conditions.

$$\text{rate} = k_{2,0}[\text{Ru}]^2 \quad (14)$$

Several variants of this pathway involving Mn^V=O and/or Mn^{IV}-oxyl have been proposed for the OEC. This was also the guiding principle behind the design of the blue dimer where two nearby Ru-oxo groups were expected to undergo O-O coupling and subsequent O₂ evolution, but it was ultimately shown to go through a single-site pathway.^{65,66}

4.2.1. Thermodynamic analysis. The chief thermodynamic considerations in the I2M O-O coupling pathway can be analyzed in a manner similar to that for the single-site WNA catalysts. Again, the goal is not to calculate a precise value for $\Delta G(\text{O-O})_{\text{I2M}}$, but rather to guide catalyst design through understanding the importance of the various thermodynamic quantities. Scheme 5 lists a thermochemical cycle linking two Ru^V=Oⁿ⁺ molecules and the resulting Ru^{IV}-O-O-Ru^{IV(2n)+} dimer.

The scheme is more complex than the WNA scheme because it involves intramolecular disproportionation of the Ru^{IV}-O-O-Ru^{IV(2n)+} dimer and the activation of two catalyst molecules, but we have the advantage of being able to use the $\Delta G(\text{O-O})_{\text{WNA}}$ from above to simplify. First, as an alternative to the overall reaction making/breaking the O-O bond between two Ru^V=Oⁿ⁺ moieties, Ru^{IV}-O-O-Ru^{IV(2n)+} can undergo intramolecular disproportionation to Ru^V-O-O-Ru^{III(2n)+}, see Section 5.2 below. Seven-coordinate Ru^{III} is unstable and de-coordination of the peroxide ligand generates the two monomeric units Ru^V-(O-O)ⁿ⁺ and Ru^{III(n)+} (reverse of step a).

Simple pathways can then be constructed from Ru^V=Oⁿ⁺ to each of these mononuclear species, using quantities that can be measured experimentally or reasonably estimated. The first

Ru^V=Oⁿ⁺ can be converted to Ru^{III(n)+} following the same pathway as in Scheme 4 (steps b-e in Scheme 5, steps a-d in Scheme 4) and then simply de-coordinating water from Ru^{III}-OH₂ⁿ⁺ (step f). The second Ru^V=Oⁿ⁺ can be converted to Ru^V-(O-O)ⁿ⁺ by first using the entire cycle in Scheme 4 to give Ru^{III}-OOH⁽ⁿ⁻¹⁾⁺ (step g, $\Delta G(\text{O-O})_{\text{WNA}}$), then going through an oxidation, a deprotonation, and another oxidation (steps h-j).

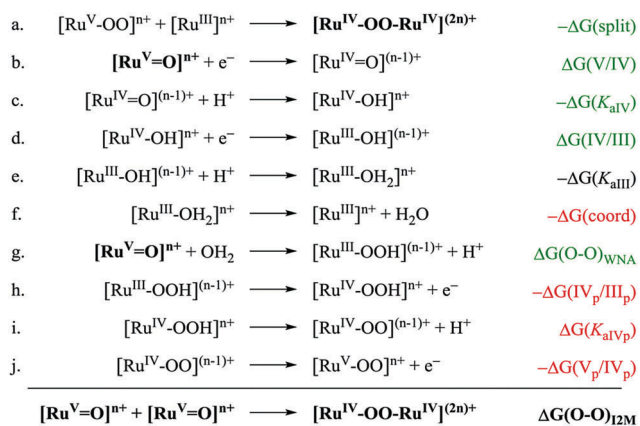
A few simple comparisons reveal that the driving forces that make up $\Delta G(\text{O-O})_{\text{I2M}}$ are more favourable than those that make up $\Delta G(\text{O-O})_{\text{WNA}}$. As discussed previously for $\Delta G(\text{III}_p/\text{II}_p)$, it can be reasonably assumed that $-\Delta G(\text{V}_p/\text{IV}_p)$ and $-\Delta G(\text{IV}_p/\text{III}_p)$ (steps h and j) are overcompensated by $\Delta G(\text{V}/\text{IV})$ and $\Delta G(\text{IV}/\text{III})$ (steps b and d). This is because the oxidation potentials for the oxo and hydroxo complexes are typically higher than the peroxy and hydroperoxy complexes, making the combination of these a favorable contributor to the driving force for O-O coupling. Second, $\Delta G(\text{p}K_{\text{aIVp}}) - \Delta G(\text{p}K_{\text{aIV}})$ (steps c and i) can be approximated based on the pK_a difference between H₂O₂ and H₂O, as above for $\Delta G(\text{p}K_{\text{aIIIp}}) - \Delta G(\text{p}K_{\text{aIII}})$. This leads to approximately an additional 0.24 eV in favor of coupling.

The factor that makes the most significant difference between the I2M and WNA pathways is $-\Delta G(\text{split})$. As discussed below in Section 5.2, the disproportionation (reverse of step a) is a likely step in the catalytic cycle that takes place after the oxidation or coupling steps that are typically rate-determining. This term can be significantly influenced by non-covalent interactions between ligands on separate fragments as discussed in Section 4.2.3. It can easily contribute up to 0.5 eV of driving force to the O-O bond formation step for catalysts with strong intermolecular interactions, and it can be highly unfavorable for catalysts with significant steric hindrance.

The remaining factors are not easily estimated, but are relatively small compared to the oxidations and $-\Delta G(\text{split})$. The coordination of water to Ru^{III(n)+} is typically spontaneous, thus $-\Delta G(\text{coord})$ will be unfavorable. As discussed in Section 3, the water coordination equilibrium constant for some catalysts is close to 1, in which case $-\Delta G(\text{coord})$ will be small. The pK_a of Ru^{III}-OH₂ⁿ⁺ also plays a role, with a less acidic aqua ligand being more favorable, but its impact will be minor considering the modest pK_a's discussed in the Section 3.2.

The thermochemical cycle can then be summarized as $\Delta G(\text{O-O})_{\text{WNA}}$ with several additional favorable contributions towards the overall driving force, $\Delta G(\text{O-O})_{\text{I2M}}$, most significantly $-\Delta G(\text{split})$. This analysis confirms what would be expected: for catalysts with favorable intermolecular interactions, the coupling of two Ru-oxos has a larger driving force compared to WNA at a single site. This is reflected in significantly higher rates and lower overpotentials for **8** and **8'** compared to **1-5**. **8** and its derivatives have favorable non-covalent interactions, and a relatively low value for $-\Delta G(\text{coord})$. As a result, $\Delta G(\text{O-O})_{\text{I2M}}$ is equal to $\Delta G(\text{O-O})_{\text{WNA}}$ with the addition of the favourable contributions mentioned above.

The conclusions for informing catalyst design are mostly the same as above but with one important addition: (1) store enough energy through the Ru^{V/IV} and Ru^{IV/III} oxidations to drive the reaction, while minimizing the difference between them, (2) take



Scheme 5 Thermochemical cycle analysing bimolecular O-O bond formation via I2M between two [Ru^V=O]ⁿ⁺ catalyst molecules. Green indicates favourable contributions and red indicates unfavourable ones.

into account non-covalent interactions between ligands that can help stabilize $\text{Ru}^{\text{IV}}\text{-O-O-Ru}^{\text{IV}(2n)+}$, as discussed in Section 4.2.3 below, (3) maximize the $\text{p}K_{\text{aIV}}$ of $[\text{Ru}^{\text{IV}}\text{-OH}]^{n+}$ and $\text{p}K_{\text{aIII}}$ of $[\text{Ru}^{\text{III}}\text{-OH}_2]^{n+}$, (4) increase the $\text{Ru}^{\text{III/II}}$ potential, and lastly (5) moderate the affinity of Ru^{III} for a water ligand. However, too much stabilization of the dimeric intermediate could result in rate limiting O_2 evolution, and an exceedingly low affinity for water will limit the rate of the oxidative activation steps.

Some catalysts will vary from the generic case in Scheme 5. Dinuclear complexes will have more complex and interwoven oxidation steps, and redox-active ligands can further muddle the oxidation states. Catalysts that can undergo O–O coupling at oxidation states lower than Ru^{V} will obey an equivalent scheme with all oxidation states lowered by one, since the same number of electrons must be transferred in this half of the catalytic cycle. Regardless, the overall principles regarding oxidation potentials and $\text{p}K_{\text{aS}}$ still apply.

4.2.2. Intramolecular O–O coupling (i-I2M). The first clear example for O–O coupling in artificial catalysts was reported by Tanaka and co-workers with the catalyst $[\text{Ru}_2(\text{OH})_2(3,6\text{-Bu}_2\text{Q})_2(\text{btpyan})]^{2+}$ (**11**, 3,6-Bu₂Q is 3,6-di-*tert*-butyl-1,2-benzoquinone; btpyan is 1,8-bis(2,2':6',2''-terpyridyl-4'-yl)anthracene), known as Tanaka's catalyst and shown in Chart 4.^{57,58} In this catalyst the catechol ligands play a non-innocent role by undergoing oxidation to the corresponding semiquinones and quinones while the oxidation state of the Ru centres remain mostly unchanged.^{55,59} The $4\text{H}^+/4\text{e}^-$ requirement for water oxidation to dioxygen is met by loss of 4H^+ from the two coordinated water molecules and loss of 4e^- from the two catecholates that undergo oxidation to the corresponding quinones. Significant

orbital overlap between the quinones and the Ru–O moieties allows hole transfer and intramolecular O–O bond formation.

Another example of intramolecular O–O coupling was provided by Llobet and co-workers with the Ru-Hbpp system *in, in*- $[\text{Ru}^{\text{II}}(\text{tpy})(\text{OH}_2)_2(\mu\text{-bpp})]^{3+}$ (**12**, bpp is bis(2-pyridyl)-3,5-pyrazolate).^{51–53} For this catalyst, successive PCET processes generate $[\text{O}=\text{Ru}^{\text{IV}}(\text{bpp})\text{Ru}^{\text{IV}}=\text{O}]^{3+}$ where the $\text{Ru}^{\text{IV}}=\text{O}$ groups with significant Ru^{III} -oxyl character are facing each other in an almost ideal position for O–O coupling. A computational study by Baik *et al.* proposed a WNA pathway for **12**.¹⁷³ The argument in favour of the WNA mechanism was based on a high barrier for O_2 evolution from the easily formed intramolecular peroxide coupling product. However, Baik and co-workers failed to explore further oxidative activation of the bridging peroxide intermediate, a common feature preceding the O_2 evolution step, or disproportionation of the peroxide intermediate. Detailed ¹⁸O-labeling studies in combination with DFT calculations by Llobet and co-workers revealed that **12** produces O_2 exclusively through the O–O coupling mechanism with a free energy of activation for this step of +15.3 kcal mol^{−1}.^{52,53}

4.2.3. Bimolecular catalysts (I2M). There are only a couple examples of bimolecular O–O coupling by Ru-based catalysts. One is *trans*- $[\text{Ru}(\text{tpym})(\text{OH}_2)_2(\mu\text{-bpp})]^{3+}$ (**13**, tpym is tris-(2-pyridyl)methane), a dinuclear complex similar to **12** shown in Chart 4, but with a facial tris-(2-pyridyl)methane ligand (tpym) in place of the equatorial tpy.¹⁴⁶ The tpym ligand enforces a geometry in which the two Ru–O units are facing away from one-another, preventing an i-I2M mechanism. Isotopic labeling studies showed that the O_2 released still originated exclusively from the Ru–O units with a second order dependence on catalyst concentration, leading to the conclusion that, in contrast to **12**, an intermolecular I2M mechanism was operative.

To the best of our knowledge, the only other example in the literature of bimolecular O–O coupling with Ru-based catalysts is the $[\text{Ru}(\text{bda})(\text{L})_2]$ systems (**8**, **8'**) initially reported by Sun and co-workers.^{60,61} These catalysts oxidize water with very high rates at pH 1.0 with Ce^{IV} as sacrificial oxidant. The TOFs, 32 s^{−1} and 300–700 s^{−1} for **8** and **8'**, respectively, have been reported with close to quantitative O_2 conversion efficiency and with thousands of turnovers.^{60,61,133} Electrochemical studies reveal almost identical potentials for the relevant oxidative couples ($\text{Ru}^{\text{III/II}}$, $\text{Ru}^{\text{IV/III}}$ and $\text{Ru}^{\text{V/IV}}$) of **8** and **8'**.⁶¹ Therefore, the difference in catalytic activity of more than an order of magnitude between the two is not due to the difference in driving forces. A combination of experimental results and DFT calculations led the authors to propose a mechanism where the key O–O bond formation step takes place by a bimolecular radical coupling of two Ru^{V} -oxo moieties with significant Ru^{IV} -oxyl radical character.^{61,63} These systems and related ones have been the subject of a great deal of further study,^{98,132,135,147,170,174,175} and we discuss them in detail here as a case study for bimolecular I2M catalysts.

The kinetics of the bda^{2−} family of catalysts are dominated by secondary interactions, reflecting their bimolecular nature.^{60,61,98} The catalysts exhibit concentration-dependent kinetics, with the rate law switching with varying catalyst concentration.⁹⁸ At low catalyst concentrations, the rate law exhibits second order

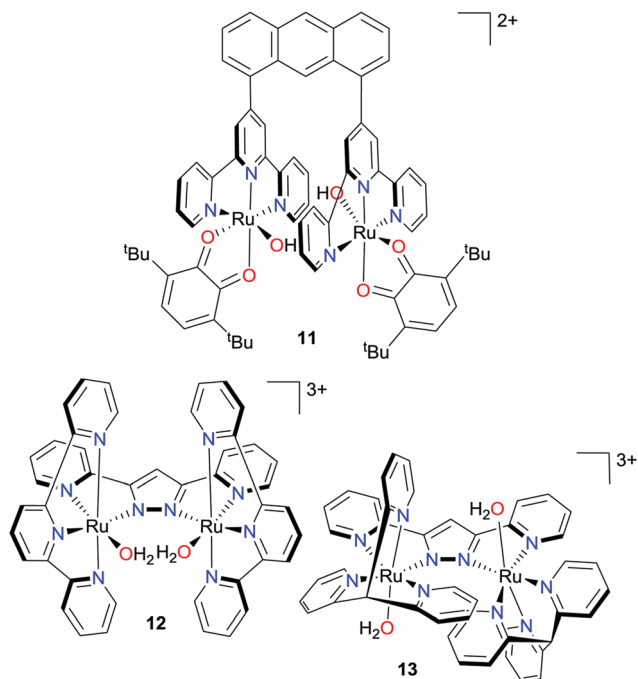


Chart 4 Chemical structures of $[\text{Ru}_2(\text{OH})_2(3,6\text{-Bu}_2\text{Q})_2(\text{btpyan})]^{2+}$ (**11**), $[\text{Ru}^{\text{II}}(\text{tpy})(\text{OH}_2)_2(\mu\text{-bpp})]^{3+}$ (**12**), and *trans*- $[\text{Ru}(\text{tpym})(\text{OH}_2)_2(\mu\text{-bpp})]^{3+}$ (**13**).

dependence on catalyst concentration and zero order dependence on Ce^{IV} concentration, indicating a rate-limiting O–O bond-forming step as shown in eqn (10) and (14). The rate of the bimolecular reaction increases with $[\text{Ru}]^2$, and eventually reaches a point where it is no longer the slow step. At higher $[\text{Ru}]$, the reaction becomes first order in both $[\text{Ce}^{\text{IV}}]$ and $[\text{Ru}]$, indicating a rate-limiting oxidation, shown in eqn (1). The rate constants $k_{1,1}$ for the slow oxidation steps at pH 1.0 are $1.8 \times 10^4 \text{ M}^{-1} \text{ s}^{-1}$ and $8.4 \times 10^4 \text{ M}^{-1} \text{ s}^{-1}$ for **8** and **8'**, respectively.⁹⁸ That they are of similar magnitude reflects the similar oxidation potentials, but they are different enough to suggest some additional advantage from the isq ligand. On the other hand, the coupling rate constant of $1.8 \times 10^7 \text{ M}^{-1} \text{ s}^{-1}$ for **8'** is almost 2 orders of magnitude greater than the $5.3 \times 10^5 \text{ M}^{-1} \text{ s}^{-1}$ for **8**.⁹⁸ This behaviour is mirrored by the vastly different TOF maxima and is consistent with the strong π – π stacking interactions in the TS between the axial isoquinolines of the two molecules, which were invoked to explain the higher catalytic activity in **8'**.⁶¹ An early study of **8'** also reported a regime that was rate-limited by oxidation of the bridging $\text{Ru}^{\text{IV}}\text{–O–O–Ru}^{\text{IV}}$ peroxide, second order in $[\text{Ru}]$ and first order in $[\text{Ce}^{\text{IV}}]$.⁶¹ It should be noted that mechanistic calculations on these systems have so far been limited to coordinate scans along the O–O distance, without locating the actual fully optimised transition state (TS) structures.^{61,63}

The presence of multiple kinetic regimes is problematic for catalyst comparison because different variants could follow different rate laws under identical conditions. Meaningful comparisons can only be made for catalysts within the same kinetic regime. Simple comparisons of TOFs may not always provide valuable lessons.

Follow-up studies by the Sun and other groups tried to improve catalytic activity with ligand modifications in the axial positions or with introduction of electron-withdrawing or electron-donating groups on the axial pyridines, shown in Chart 5.^{133,134,176} The best results were obtained with 6-fluoroisoquinoline (TOF = 1000 s^{-1}) replacing isoquinoline (TOF = 800 s^{-1}) as the axial ligand.¹³³ Llobet and co-workers studied the interactions between the axial ligands in $[\text{Ru}(\text{bda})(\text{L})_2]$ (L is 6-methoxyisoquinoline, **14**, and positively-charged 1-methyl-4,4'-bipyridinium, **15**) in more detail.¹⁴⁷ They studied catalytic activity for **14**, **15** and an equimolar mixture of **14** and **15**. In addition, the authors also located TS structures at the M06L level, although in the gas phase, and extracted quantitative information about L–L interactions in the TS structures. The order obtained for the L–L interaction energy was **14–14** > **14–15** >> **15–15**, in agreement with the experimental results.

Despite the number of reports investigating the effects of axial ligands and substituents, conclusive guidelines for catalyst design has been lacking, with some studies changing several variables at once.¹³⁴ For example, Ahlquist *et al.*¹⁴⁰ reported DFT studies on $[\text{Ru}(\text{bda})(4\text{-X-py})_2]$ (X is –H, –Br, –Me, –COOEt, –OMe, –NMe₂) and $[\text{Ru}(\text{bda})(6\text{-X-isq})_2]$ (X is –H, –F) and compared their findings with available experimental data for these catalysts from previous reports. They found no correlation between electronic activation barriers (no TS calculations

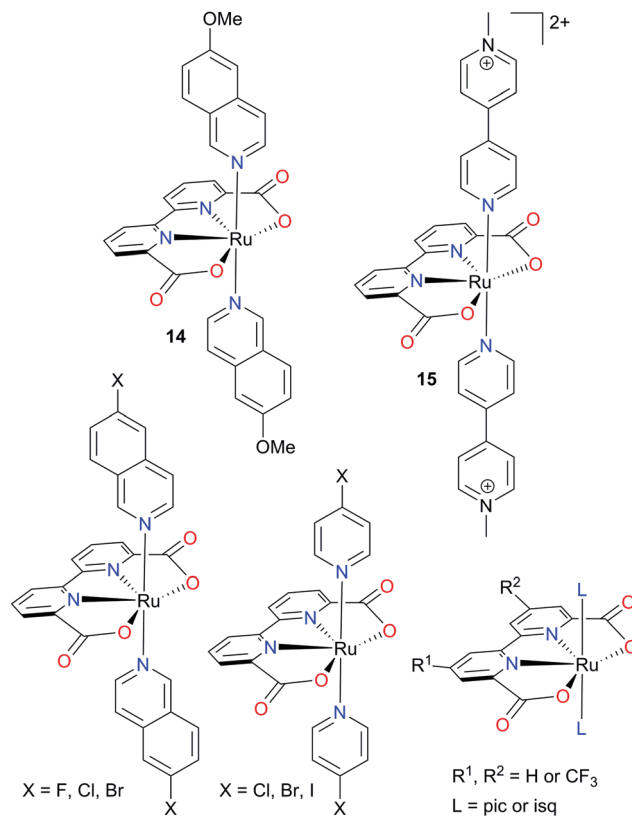


Chart 5 Chemical structures for variants of the $[\text{Ru}(\text{bda})(\text{L})_2]$ catalyst system, including variable axial ligands (L is 6-methoxyisoquinoline in **14**, positively-charged 1-methyl-4,4'-bipyridinium in **15**, 6-haloisoquinolines, and 4-halopyridines) and the more electron withdrawing 4- CF_3 -bda²⁻ and 4,4'-(CF_3)₂-bda²⁻.

were carried out) and the structure of the axial ligands. They also reported that electron-withdrawing groups improved catalytic activity. Similar conclusions were reached by Sun and co-workers with respect to electron-withdrawing groups but they also concluded that electron-donating groups had a negative effect on catalysis.¹³⁴ Experimental results reported by Murata and co-workers¹⁷⁶ for $[\text{Ru}(\text{bda})(4\text{-X-py})_2]$ (X is –H, –Br, –Me, –COOMe, –OMe, –CF₃) were also inconclusive, and included some conflicting results. Hammett analysis demonstrated that the catalytic activities of the complexes toward chemical and photochemical water oxidation showed no straightforward dependence on the electronic nature of the substituent group, with both donating and withdrawing groups able to accelerate catalysis relative to the parent pyridine complex.¹⁷⁶

We designed two separate systematic studies to gain a clear understanding of the key mechanistic features for these catalysts. Selected results are summarized in Table 3. In one study, the axial ligands were kept the same as in the original **8** and **8'** systems and one or two electron-withdrawing trifluoromethyl groups were introduced in the 4 and 4' positions of the bda backbone.⁹⁸ The goal was to study the effect of redox potentials of different couples on catalytic activity while maintaining the same interaction energy between the axial ligands. Since the $\text{Ru}^{\text{V}}\text{=O}$ group is located in the equatorial plane, it was

anticipated that the most influential adjustments would be in the backbone of the tetradentate bda²⁻ ligand. The series [(4-R¹,4'-R²-bda)Ru(L)₂] (R¹ and R² are -H or -CF₃ and L is 4-picoline or isoquinoline) comprised three catalysts for each axial ligand with six complexes in total. As expected, changes in oxidation potentials were observed. The increase in redox potential is 70–80 mV per CF₃ group for Ru^{III/II} couple and 20–30 mV per CF₃ group for Ru^{IV/III} couple.⁹⁸ The lesser effect on the higher oxidation state potentials is consistent with less overlap between the π system of the ligand and the smaller, less populated d-orbitals of the more highly oxidized Ru. Careful kinetic studies using stopped-flow kinetics at pH 1.0 with Ce^{IV} as sacrificial oxidant allowed observation of both kinetic regimes mentioned above for all six catalysts. To our surprise, the additional electron withdrawing groups had only a minor influence on both the bimolecular rate constant, $k_{2,0}$, and even the oxidation rate constant, $k_{1,1}$.⁹⁸ The relatively small variance in $k_{1,1}$ reflects the lesser differences found in the Ru^{IV/III} potentials. Further oxidation to Ru^V, which may be rate-determining, is likely to feel an even weaker influence from the substituents. Considering the minor impact of the CF₃ groups on the oxidation rate constant, the trivial electronic influence on the bimolecular oxo/oxyl coupling rate constant $k_{2,0}$ is no surprise. These results are consistent with this step being primarily dictated by secondary interactions between catalyst molecules.

For our second study, we focused our attention on the axial ligands, examining systematic changes throughout two series of halogen-substituted ligands.¹³⁵ We first looked at the halides as substituents in the 4 and 6 positions of pyridine and isoquinoline, respectively, while keeping the parent bda²⁻ backbone. The series [(bda)Ru(4-X-py)₂] (X is H, Cl, Br, I) and [(bda)Ru(6-X-isq)₂] (X is H, F, Cl, Br) were prepared. Non-covalent interactions between the halogens in the TS are expected to increase from fluorine to iodine as they become more polarizable. For each catalyst, $k_{2,0}$ and $k_{1,1}$ were determined at pH 1.0 using stopped-flow kinetics. We also located O–O coupling TS structures and calculated activation parameters for all catalysts in the two series, as well as the interaction energy between the axial ligands in the TS structures.

Calculated free energies of activation, ΔG^\ddagger , and experimental rate constants, $k_{2,0}$, followed a clear trend with more favourable ligand–ligand interactions leading to more facile coupling. Calculated values of ΔG^\ddagger were always significantly lower for members of the isoquinoline series compared to their corresponding pyridine analogues. This is consistent with experimental rates and in contrast with the results reported by Ahlquist *et al.*¹⁴⁰ For both series, the entropic term $-T\Delta S^\ddagger$ was the dominant contributor to ΔG^\ddagger with negative ΔH^\ddagger for all members of the two series except L = pyridine. Plots of $\ln(k_{2,0})$ vs. ΔG^\ddagger for each series displayed a linear relationship according to the Eyring equation. This result is noteworthy considering ΔG^\ddagger comes from DFT calculations and $k_{2,0}$ comes from experimental measurements. Rate constants for the pyridine series increased more than 20 times from $3.1 \times 10^5 \text{ M}^{-1} \text{ s}^{-1}$ for X = -H to $7.7 \times 10^6 \text{ M}^{-1} \text{ s}^{-1}$ for X = -I.

For the isoquinoline series the changes were more moderate. But careful analysis of the TS structure for **8'** led us to introduce electron-donating groups on the phenyl ring of isoquinoline to enhance π - π stacking interactions. We added the complexes with L = 6-OMe-isq and L = 6,7-(OMe)₂-isq to the isoquinoline series and once again our theoretical predictions were proven right: $k_{2,0}$ increased from $1.8 \times 10^7 \text{ M}^{-1} \text{ s}^{-1}$ for L = isq to $1.2 \times 10^8 \text{ M}^{-1} \text{ s}^{-1}$ for L = 6-OMe-isq and to $3.4 \times 10^8 \text{ M}^{-1} \text{ s}^{-1}$ for L = 6,7-(OMe)₂-isq, corresponding to about 7 and 20 times enhancement, respectively, with respect to the parent catalyst. This is once again in complete contrast with previous studies reporting that electron-donating groups had a negative effect on catalytic activity.¹³⁴

It is quite remarkable that for [Ru(bda)(L)₂] the catalytic activity is determined almost exclusively by the non-covalent interactions between the axial ligands. The calculated ligand–ligand interaction energies correlated very well with ΔG^\ddagger and more specifically with ΔH^\ddagger . The effect of these interactions is to compensate the high entropic penalty associated with a highly organized TS, and in doing so, to lower ΔG^\ddagger for intermolecular O–O bond formation. Minor ligand modifications led to an increase in TOF from 22 s^{-1} for [Ru(bda)(py)₂] to 330 s^{-1} for [Ru(bda)(4-I-py)₂] and from 660 s^{-1} for [Ru(bda)(isq)₂] to 1270 s^{-1} for [Ru(bda)(6-OMe-isq)₂].¹³⁵ These results show the value of careful and systematic mechanistic studies combining experiments and DFT calculations.

5. O₂ evolution

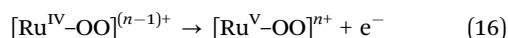
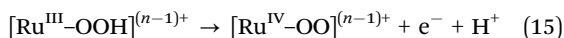
The last step of the water oxidation cycle involves ³O₂ being evolved and the catalyst re-entering the catalytic cycle. Compared to the O–O bond formation step, the oxygen evolution step is significantly less demanding from a free energy point of view. But in most cases one or more oxidative activation steps are required between O–O bond formation and O₂ evolution, often with the requirement for a proton loss. In addition, the O₂ evolution step can involve a coordination contraction from seven- to six-coordinate species with re-coordination of one or two water molecules through associative or dissociative mechanisms. If not properly addressed, these mechanistic complications can become rate limiting. However, in most cases, all steps following O–O bond formation are faster than the previous steps, making experimental studies difficult and requiring more reliance on calculations.

5.1. Single-site catalysts

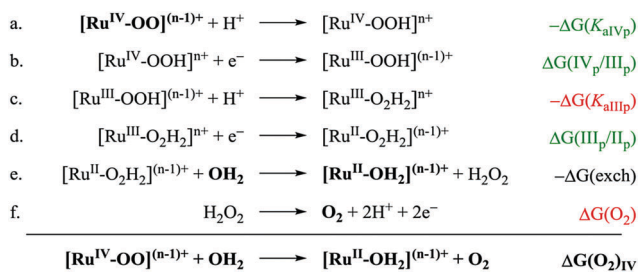
For Ru-based single-site catalysts, O₂ evolution takes place from six- or seven-coordinate ³[Ru^{IV}(η^1 -OO)]⁽ⁿ⁻¹⁾⁺ or ²[Ru^V(η^1 -OO)]ⁿ⁺.^{69,70,116,124,126} For the six-coordinate systems (**1–5**), DFT calculations suggest the open form of the peroxide (end-on) is in equilibrium with seven-coordinate ¹[Ru^{IV}(η^2 -OO)]⁽ⁿ⁻¹⁾⁺ or ²[Ru^V(η^2 -OO)]ⁿ⁺ (side-on peroxide).^{69,70,116,117} Although the side-on isomers are believed to be more stable,¹⁷⁷ interconversion between the two is not expected to be rate-limiting.¹¹⁷ The doublet ²[Ru^V(η^2 -OO)]ⁿ⁺ can be also envisioned as a loosely

bound $\{^2[\text{Ru}^{\text{III}}]^{-3}\text{O}_2\}^{n+}$ complex that is weakly antiferromagnetically coupled, with $^4[\text{Ru}^{\text{V}}(\eta^1\text{-OO})]^{n+}$ usually being higher in energy. Oxygen evolution from $^3[\text{Ru}^{\text{IV}}(\eta^1\text{-OO})]^{(n-1)+}$ yields $^3\text{O}_2$ and $^1[\text{Ru}^{\text{II}}]^{(n-1)+}$ or $^1[\text{Ru}^{\text{II}}\text{-OH}_2]^{(n-1)+}$ and from $^2[\text{Ru}^{\text{V}}(\eta^1\text{-OO})]^{n+}$ yields $^3\text{O}_2$ and $^2[\text{Ru}^{\text{III}}]^{n+}$, $^2[\text{Ru}^{\text{III}}\text{-OH}]^{(n-1)+}$, or $^2[\text{Ru}^{\text{III}}\text{-OH}_2]^{n+}$.

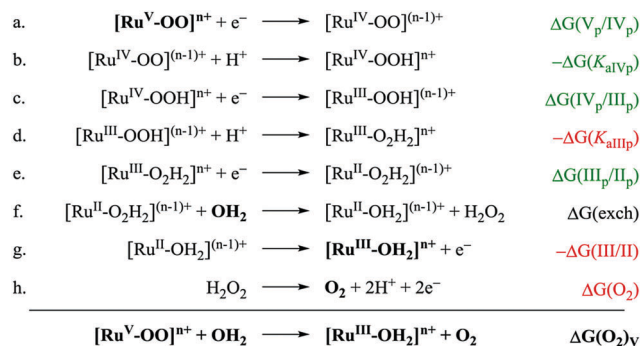
The initial intermediate after O–O bond formation is $\text{Ru}^{\text{III}}\text{-OOH}^{n+}$, and oxidative activation is required before O_2 can be evolved, eqn (15) and (16). Thermodynamically, the free energy requirements for the processes in eqn (15) and (16) are less demanding than for the corresponding $\text{Ru}^{\text{V/IV}}$ and $\text{Ru}^{\text{IV/III}}$ couples for the aqua complexes. This could be rationalized again in terms of the difference in $\text{p}K_{\text{a}}$ values of 4 units between H_2O and H_2O_2 . Assuming $E_{1/2}(\text{Ru}^{\text{III}}\text{-OH}_2^{3+}/\text{Ru}^{\text{II}}\text{-OH}_2^{2+}) \approx E_{1/2}(\text{Ru}^{\text{III}}\text{-O}_2\text{H}_2^{3+}/\text{Ru}^{\text{II}}\text{-O}_2\text{H}_2^{2+})$ and $\text{p}K_{\text{a}}(\text{Ru}^{\text{III}}\text{-O}_2\text{H}_2^{3+}) - \text{p}K_{\text{a}}(\text{Ru}^{\text{III}}\text{-OH}_2^{3+}) \approx 4$, the redox potentials for the pH-dependent couples of the peroxide should be approximately 0.24 V lower than the corresponding aqua couples. This translates into a free energy decrease of 0.24 eV per electron and it has been corroborated experimentally for **2**¹¹⁵ and its analogue $[\text{Ru}(\text{Mebimpy})(\text{bpm})(\text{OH}_2)]^{2+}$.¹¹⁶ In addition, the redox couples involving the peroxide intermediates receive a higher contribution from electron density being removed from the peroxide itself while the aqua/hydroxo/oxo couples are more localized on the Ru center. Nevertheless, it should be noted that the redox process in eqn (15) is proton-coupled and kinetically accelerated by i-PCET.



5.1.1. Thermodynamic analysis. The need for oxidative activation of the hydroperoxide species prior to O_2 evolution is easily realized from a thermodynamic analysis for this process. Scheme 6 shows such an analysis for O_2 evolution from $\text{Ru}^{\text{IV}}\text{-OO}^{(n-1)+}$. Most of the free energy in favour of this process comes from the PCET oxidation from eqn (15). $-\Delta G(K_{\text{aIVp}})$ and $\Delta G(\text{IV}_p/\text{III}_p)$ (steps a and b) need to be sufficient to compensate $\Delta G(\text{O}_2) = +1.40$ eV from eqn (8) (step f). The protonation free energy $-\Delta G(K_{\text{aIIIp}})$ (step c) is positive (+0.1–0.24 eV) and will have a negative impact on the overall $\Delta G(\text{O}_2)_{\text{IV}}$. Without the contribution from $\Delta G(\text{IV}_p/\text{III}_p)$, there is not enough free energy to compensate $\Delta G(\text{O}_2)$ because $\Delta G(\text{III}_p/\text{II}_p)$ (step d) is usually less negative than -1.0 eV and $\Delta G(\text{exch})$ is



Scheme 6 Thermodynamic cycle for oxygen evolution from single-site ruthenium catalysts from $\text{Ru}^{\text{IV}}\text{-OO}^{(n-1)+}$. Green indicates favourable contributions and red indicates unfavourable ones.



Scheme 7 Thermodynamic cycle for oxygen evolution from single-site ruthenium catalysts from $\text{Ru}^{\text{V}}\text{-OO}^{n+}$. Green indicates favourable contributions and red indicates unfavourable ones.

again anticipated to be small and have a minor contribution. Using available experimental data for catalyst **2**, we obtain a slightly unfavourable $\Delta G(\text{O}_2)_{\text{IV}} \approx +0.30$ eV (+6.9 kcal mol⁻¹), assuming $\Delta G(\text{exch}) = 0$.¹¹⁵

Another important feature that emerges from the thermodynamic analyses for O–O bond formation and for O_2 evolution is that some of the contributors to the free energy appear in both processes with opposite signs (*e.g.* $\Delta G(\text{III}_p/\text{II}_p)$). This implies that some of the factors that favour O–O bond formation work against O_2 evolution, and *vice versa*.

A similar analysis for O_2 evolution from $\text{Ru}^{\text{V}}\text{-OO}^{(n+1)+}$ is shown in Scheme 7. In this case, the contribution from $\Delta G(\text{III}_p/\text{II}_p)$ (step e) is offset by $-\Delta G(\text{III}/\text{II})$ (step g), but there is additional contribution from $\Delta G(\text{V}_p/\text{IV}_p)$ (step a) which is usually more negative than -1.0 eV since $E_{1/2}$ for this couple is usually above +1.0 V. Therefore, O_2 evolution from $\text{Ru}^{\text{V}}\text{-OO}^{n+}$ is more favourable than from $\text{Ru}^{\text{IV}}\text{-OO}^{(n-1)+}$ by $\Delta G(\text{V}_p/\text{IV}_p) - \Delta G(\text{III}/\text{II})$. If the $\text{p}K_{\text{aIII}}$ of $\text{Ru}^{\text{III}}\text{-OH}_2^{n+}$ is low and $\text{Ru}^{\text{III}}\text{-OH}^{(n-1)+}$ is the more stable form, an additional contribution from $\Delta G(K_{\text{aIII}})$ favours O_2 release. For catalyst **2** we obtain $\Delta G(\text{O}_2)_{\text{V}} \approx -0.17$ eV (-3.9 kcal mol⁻¹),¹¹⁵ assuming $\Delta G(\text{exch}) = 0$, a gain of 0.47 eV in favour of O_2 evolution from $\text{Ru}^{\text{V}}\text{-OO}^{n+}$ compared to $\text{Ru}^{\text{V}}\text{-OO}^{(n-1)+}$. Notably, $\Delta G(\text{O}_2)_{\text{V}}$ is also more favourable than $\Delta G(\text{O-O})_{\text{WNA}} \approx -0.06$ eV for O–O bond formation for the same catalyst, reinforcing the key role of the latter in water oxidation.

Aside from thermodynamic considerations, there are important advantages for catalysts **9** and **10** compared to **1–5** when it comes to O_2 evolution. For catalysts **1–5** the final step takes place from a six-coordinate $^3[\text{Ru}^{\text{IV}}(\eta^1\text{-OO})]^{2+}$ or $^2[\text{Ru}^{\text{V}}(\eta^1\text{-OO})]^{3+}$ and the catalyst ends as six-coordinate $^1[\text{Ru}^{\text{II}}\text{-OH}_2]^{2+}$, $^2[\text{Ru}^{\text{III}}\text{-OH}]^{2+}$, or $^2[\text{Ru}^{\text{III}}\text{-OH}_2]^{3+}$.^{69,116,117} An associative mechanism would involve a highly organized, sterically crowded seven-coordinate TS, in which both the incoming water molecule and the leaving O_2 are partially bound to the Ru centre, imposing an entropic penalty on ΔG^\ddagger . If the final product is $^2[\text{Ru}^{\text{III}}\text{-OH}]^{2+}$, the requirement for a proton loss introduces an additional mechanistic complication. On the other hand, a dissociative mechanism will generate high energy five-coordinate $\text{Ru}^{\text{II}(2+)}$ or $\text{Ru}^{\text{III}(3+)}$ intermediates that will impose an enthalpic penalty upon ΔG^\ddagger . For catalysts **9** and **10**, the wide angle tetradentate ligands allow for stable seven-coordinate complexes. O_2 evolution takes place from

seven-coordinate $^3[\text{Ru}^{\text{IV}}(\eta^1\text{-OO})]^{(n-1)+}$ or $^2[\text{Ru}^{\text{V}}(\eta^1\text{-OO})]^{n+}$ and the catalyst ends as six-coordinate $^1[\text{Ru}^{\text{II}}]^{(n-1)+}$ or $^2[\text{Ru}^{\text{III}}]^{n+}$, without water in the coordination environment.^{124,126} They follow a more facile dissociative mechanism because there is no need for a five-coordinate intermediate.

5.2. Two-site I2M catalysts

O₂ evolution from bridging peroxides has not been studied in detail, regardless of whether the peroxide is the only ligand connecting the two metal centres or another bridging ligand (BL) exists in addition to the peroxide. Experimentally, these studies have been difficult because the steps following O–O bond formation are often faster than the rate-limiting step. Computationally, these studies are more costly because of the size of the dinuclear systems compared to single-site catalysts.

Llobet and co-workers proposed a mechanism for **12** including O₂ evolution from the Ru^{III}–O–O–Ru^{III} peroxide intermediate.⁵² This process can occur by direct release of dioxygen or through an associative mechanism in which water displaces the peroxide from one of the metal centres. The mechanism proposed by Llobet and co-workers involves water attack on one of the six-coordinate Ru centres through an associative seven-coordinate TS. In the product HOO–Ru^{III}(BL)Ru^{III}–OH, one of the protons of the incoming water molecule has been transferred to the peroxide that now is bound to only one Ru centre as a terminal hydroperoxide. O₂ evolution from this point is analogous to single-site catalysis.

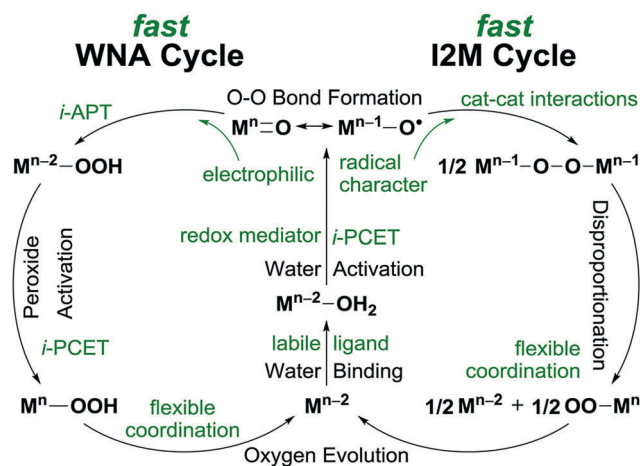
In the case of catalyst **8**, such an associative mechanism is unlikely. The product of O–O coupling for this catalyst is a Ru^{IV}–O–O–Ru^{IV} peroxide where both Ru centres are seven-coordinate. This inhibits water attack on these centres. Direct O₂ evolution from Ru^{IV}–O–O–Ru^{IV} or further oxidized Ru^V–O–O–Ru^{IV} to simultaneously generate three molecules is also unlikely. A more plausible scenario is through intramolecular disproportionation from Ru^{IV}–O–O–Ru^{IV} to Ru^{III}–O–O–Ru^V. Seven-coordinate Ru^{III} is unstable and de-coordination of the peroxide ligand generates two monomeric units: six-coordinate Ru^{III} and seven-coordinate Ru^V–OO. Oxygen evolution from the latter can follow as in the single-site O₂ evolution process discussed above for **9** and **10**. This pathway is currently being explored with DFT calculations.

6. Catalyst design

6.1. Summary of catalyst optimization strategies

The previous sections have shown with selected examples that thoughtful catalyst design can manipulate the favourability of each step in water oxidation catalysis and improve overall catalytic rates. Detailed kinetic studies elucidating the operative mechanism and rate-determining step allow for appropriate adjustments to be made in future studies. Scheme 8 outlines the two major mechanisms for WOC and includes factors that facilitate each step.

Oxidative activation steps require facile water coordination and PCET oxidations. For catalysts which are coordinatively



Scheme 8 Overview of water nucleophilic attack (WNA) and oxo-oxo coupling (I2M) mechanisms for water oxidation catalysis, with strategies for facilitating the various steps in green.

saturated before water binding, this step can be facilitated by multidentate ligands with labile groups that can de-coordinate to allow a water molecule into the coordination sphere. Such is the case for catalysts **8** and **10**, in which a carboxylate group is labile enough in the Ru^{III} state.¹²⁶ This is in contrast to related catalyst **9**, whose phosphonate ligands are more tightly bound and does not bind water until it reaches Ru^{IV}. Llobet and coworkers have also utilized this strategy in a complex similar to **8**, but with a tpy backbone instead of bpy, [Ru(tda)(py)₂] (tda²⁻ is [2,2':6',2''-terpyridine]-6,6''-dicarboxylate, py is pyridine).¹²⁷

The steps to oxidatively activate the metal-bound water molecule to reach a reactive Ru=O can be accelerated in a couple of different ways. Oxidations associated with proton loss can be accelerated by a properly positioned base. Uncoordinated carboxylate groups such as those in **8**, **10**, and [Ru(tda)(py)₂] are oriented to hydrogen bond with a metal-bound water molecule, ready for a fast i-PCET oxidation. Slow oxidation steps have also been shown to benefit from the use of a redox mediator with very fast intermolecular electron-transfer rates, such as [Ru(bpy)₃]²⁺. This has been demonstrated for both WNA catalysts (e.g., **3**)¹⁵⁸ and I2M catalysts (e.g., **8**).^{174,178}

There is another important aspect to be considered in the oxidative activation of the metal-bound water molecule: anation of Ru^{III}–OH₂ⁿ⁺. This deleterious process can delay or even prevent access to the required higher oxidation states in the catalytic cycle. There are three ways to circumvent or alleviate this process: (1) use ligands with strong π-accepting or electron-withdrawing capabilities to decrease pK_{a,HB}, making Ru^{III}–OH⁽ⁿ⁻¹⁾⁺ the dominant form in solution, (2) significantly increase the electron density on the Ru centre with strong σ donors to decrease affinity of Ru^{III}–OH₂ⁿ⁺ for anions, and (3) increase ligand exchange rates at the active site to prevent anion release from being rate limiting.¹¹⁸ This can be accomplished with *trans* effects or by introducing bulky groups in close proximity to the active site.

The key to accelerating the APT O–O bond-forming step in the WNA mechanism for electrophilic Ru^V=O's is mediating

the proton transfer from the incoming water molecule. Bases in solution have been shown to accelerate this step,⁷⁰ but it is most effectively done with a pre-positioned base as a part of the catalyst molecule. This strategy is operative in $[\text{Ru}(\text{tda})(\text{py})_2]$ at moderate to basic pH¹²⁷ and in **9** even at pH 1.¹²⁴ Though the pendant base in **9** allows for fast i-APT in the O–O bond-forming step, the more tightly coordinating bpa^{4-} ligand prevents water binding at Ru^{III} , preventing the aforementioned i-PCET oxidations mediated by the bda^{2-} ligand in **8**. This led to the design of **10**, in which the hybrid $\text{bda}^{2-}/\text{bpa}^{4-}$ ligand bpc^{3-} retains both the fast i-APT O–O bond formation from the pendant phosphonate and the fast i-PCET catalyst oxidative activation from the carboxylate. This design, driven by detailed mechanistic understanding, led to the development of the fastest low-pH, single site water oxidation catalysts known to date.¹²⁶

On the other hand, I2M catalysts benefit from favourably positioning the two $\text{Ru}=\text{O}$ units to form an O–O bond between them. Improving mononuclear catalysts such as **8** must be done by optimizing secondary interactions between individual catalyst molecules in the key bimolecular step.¹³⁵ This is clearly illustrated in studies involving series of **8** and **8'** with various substituents in the 4- and 6-positions of the pyridine and isoquinoline ligands, respectively. Experimental rate constants and calculated activation barriers both corroborate the more favourable secondary interactions leading to faster coupling.¹³⁵ Dinuclear I2M catalysts have lower entropic barriers because they do not require a bimolecular step, but the O–O coupling step is sensitive to the positioning of the two active sites. Rigid ligand frameworks restrict the metal centres' mobility and thus dictate the mechanism,¹⁷⁹ seen in the comparison of related catalysts **12** and **13**, which go through I2M and WNA pathways, respectively.¹⁴⁶ Thoughtful ligand design can place the active sites for optimal coupling.^{54,180} More flexible assemblies linking fragments resembling mononuclear catalysts allow the two sites to interact more freely and still reduce the entropic barrier. Such systems linking units of **8** have been effective (TOFs up to 40 s^{-1}),^{105,181} but have so far been unable to reproduce the higher TOFs reached by the mononuclear derivatives of **8'** ($> 1000 \text{ s}^{-1}$).^{133,135}

An important component of catalyst optimization for both types of catalyst is the driving force for O–O bond formation and the factors that affect it, as discussed in Section 4. For all catalysts, a large fraction of the driving force comes from the two oxidations approaching the O–O bond-forming step, typically $E_{1/2}(\text{V}/\text{IV})$ and $E_{1/2}(\text{IV}/\text{III})$. Ideally, these are very close in potential and just high enough to drive the reaction.

The $\text{Ru}-\text{OOH}$ resulting from WNA or disproportionation of a $\text{Ru}-\text{O}-\text{O}-\text{Ru}$ dimer must be oxidatively activated to provide the driving force for favourable release of O_2 . As in the case of the initial oxidation steps, these are accelerated by i-PCET, available to **9** and **10**, with a pendant phosphonate positioned to hydrogen bond with the hydroperoxide proton and relay it from the active site.

O_2 release can occur by either an associative or dissociative mechanism, concomitantly with two-electron reduction of the metal centre. This process is more favourable for systems that

can avoid unstable intermediates: crowded 7-coordinate species in associative mechanisms or high-energy 5-coordinate species in dissociative mechanisms. This is difficult for traditional octahedral catalysts such as **1–5**. Catalysts **8–10** have ligands with wide bite angles that allow them to access stable 7-coordinate $\text{Ru}^{\text{V}}-\text{OO}$ species, which can simply dissociate O_2 to form a stable 6-coordinate Ru^{III} complex.

6.2. Solution vs. surface activity

An important aspect regarding water oxidation with homogeneous catalysts in solution is how their catalytic activity translates to the corresponding “heterogenized” version with the catalyst immobilized on an electrode surface.^{74,115} This is particularly relevant for potential applications in artificial photosynthesis and electrosynthesis, for which the catalyst must be integrated on the surface of an electrode. Photochemical and photoelectrochemical applications additionally require incorporation with chromophores and/or semiconductors to serve the function of photoanode. In addition to catalytic activity, there are other aspects that need to be considered when it comes to integration: Is the catalyst amenable to incorporation into chromophore-catalyst assemblies? Can anchoring groups be easily introduced in the catalyst structure? Can they be co-loaded with chromophores? Are anchoring groups, linking groups, and assemblies stable during catalysis? Are the different intermediates of the catalyst competing with the chromophores for light absorption? Is catalytic activity maintained on the surface? Is the same mechanism operative in solution and on the surface?

Bimolecular catalysts such as **8** and **8'** are among the most active towards water oxidation in solution with very low overpotentials. They are easily functionalized with anchoring groups, typically acidic or aromatic groups attached to the axial ligands, and are also amenable for incorporation into chromophore-catalyst assemblies, e.g. tethering the axial ligands to a $\text{Ru}(\text{bpy})$ -based photosensitizer.^{148,170,182–189} In addition, most of the intermediates in the catalytic cycle are poor absorbers, making detrimental light absorption by the catalyst a minimal issue with these catalysts.

Unfortunately, the requirement of two catalyst molecules having to interact in a very specific arrangement for fast bimolecular O–O bond formation restricts the ability of $\text{Ru}-\text{bda}$ catalysts to function in surface-bound conditions.¹⁷⁰ While in solution the high entropy penalty is offset by favourable secondary interactions, this is largely prevented for site-isolated catalyst molecules, except a small fraction of which have the right orientation for bimolecular O–O bond formation. The bda^{2-} catalysts have a much higher barrier for single-site catalysis.^{124,126} As a result, the catalytic activity of bda^{2-} -based catalysts is severely inhibited when anchored to a surface.

Multinuclear catalysts that oxidize water *via* intramolecular O–O bond formation, such as **11** and **12**, are not as active as the bda^{2-} family, but their pre-positioned nature allows them to retain their solution activity when immobilized.^{57,58,190} Their drawback is the synthetic difficulty when it comes to incorporation into chromophore-catalyst assemblies or even the introduction of functional groups for anchoring purposes.

Their overpotentials are also significantly higher than for [Ru(bda)(L)₂]. In addition, these catalysts are typically strong light absorbers, even in the high oxidation states of the catalyst, due to their highly conjugated ligand frameworks and strong coupling across the bridge.

Single-site catalysts such as **1**–**5** have several advantages for the purpose of electrode immobilisation. Their synthesis is much simpler, making them amenable to incorporation into chromophore-catalyst assemblies or to functionalization with anchoring groups.^{115,158,165,191–200} Light absorption by the species involved in the catalytic cycle is very poor and, most importantly, their catalytic activity is retained on surfaces.^{115,194} They typically have two major drawbacks: their catalytic activity is relatively poor, and catalysis takes place at high overpotentials.

The design of catalysts **9** and **10** addresses the drawbacks of typical polypyridyl–Ru single site catalysts such as **1**–**5**, and are expected to perform accordingly in upcoming surface studies. The multifunctional bpaH₂²⁻ ligand in **9** and **9'** lead to improved activity by reducing the entropic barrier in the TS.¹²⁴ Introduction of the i-APT pathway led to significant enhancements in TOFs but they still fell short of the required rates and display very high overpotentials. Hybrid bpcH²⁻ catalysts **10** and **10'** retain the i-APT pathway provided by the phosphonate group from **9** and **9'**, and the labile carboxylate group enables i-PCET pathways to take place in the oxidative water activation steps, thereby reducing the overpotential.¹²⁶ **10** and **10'** achieve by far the highest TOFs of any single-site catalyst at pH 1.0, and rival those of bimolecular **8** and **8'** and the OEC. Their overpotentials are 200 mV lower compared to **9** and **9'**, although still higher than **8** and **8'**. It remains to be seen how well they perform when isolated on an electrode surface or incorporated into a dye-sensitised photoelectrosynthesis cell (DSPEC).

7. Conclusions

O–O bond formation is the key step in water oxidation catalysis. This first half of the reaction accounts for at least 70% of the free energy requirement to carry out this reaction and catalytic rates are often limited by this step. Detailed mechanistic understanding of how it takes place is paramount for the development of efficient water oxidation catalysts. Furthermore, other stages of the water oxidation cycle such as catalyst oxidative activation and oxidative activation of peroxide or hydroperoxide intermediates also have to be considered. Intramolecular or bimolecular O–O coupling provides an efficient pathway for the key O–O bond formation step and catalysts following this mechanism are among the best artificial water oxidation catalysts known to date. But careful consideration must be taken when trying to incorporate these catalysts into solar cell devices, particularly bimolecular ones since their catalytic activity is severely inhibited when site-isolated on an electrode surface.

The origination of the single-site WNA/APT mechanism in 2008 by Meyer and co-workers opened the door for the

systematic study of water oxidation catalysts following this pathway. One important aspect of this mechanism is the requirement for a proton loss in the O–O bond formation step. This realization led to the introduction of strategically positioned proton acceptor groups as part of the structure of the catalyst enabling the low activation energy i-APT pathway. Hybrid catalysts combine this pathway with low barrier i-PCET pathways in oxidative water activation and oxidative activation of peroxide or hydroperoxide intermediates to carry out efficient single-site water oxidation catalysis. They represent a promising platform for artificial photosynthesis and may provide mechanistic insight and support in favour of a WNA mechanism in the OEC.

Conflicts of interest

There are no conflicts to declare.

Acknowledgements

This work was carried out at Brookhaven National Laboratory and it was supported by the U.S. Department of Energy, Office of Science, Division of Chemical Sciences, Geosciences, & Biosciences, Office of Basic Energy Sciences under contract DE-SC00112704.

Notes and references

- 1 M. Graetzel, *Acc. Chem. Res.*, 1981, **14**, 376–384.
- 2 A. J. Bard and M. A. Fox, *Acc. Chem. Res.*, 1995, **28**, 141–145.
- 3 J. J. Concepcion, R. L. House, J. M. Papanikolas and T. J. Meyer, *Proc. Natl. Acad. Sci. U. S. A.*, 2012, **109**, 15560–15564.
- 4 W. Song, Z. Chen, M. K. Brennaman, J. J. Concepcion, A. O. T. Patrocinio, N. Y. M. Iha and T. J. Meyer, *Pure Appl. Chem.*, 2011, **83**, 749–768.
- 5 J. Su and L. Vayssieres, *ACS Energy Lett.*, 2016, **1**, 121–135.
- 6 N. S. Lewis, *Science*, 2016, **351**, aad1920.
- 7 D. G. Nocera, *Acc. Chem. Res.*, 2017, **50**, 616–619.
- 8 T. J. Meyer, *Acc. Chem. Res.*, 1989, **22**, 163–170.
- 9 R. J. Detz, K. Sakai, L. Spiccia, G. W. Brudvig, L. Sun and J. N. H. Reek, *ChemPlusChem*, 2016, **81**, 1024–1027.
- 10 D. Gust, T. A. Moore and A. L. Moore, *Acc. Chem. Res.*, 2009, **42**, 1890–1898.
- 11 S. Berardi, S. Drouet, L. Francas, C. Gimbert-Surinach, M. Guttentag, C. Richmond, T. Stoll and A. Llobet, *Chem. Soc. Rev.*, 2014, **43**, 7501–7519.
- 12 D. Kim, K. K. Sakimoto, D. Hong and P. Yang, *Angew. Chem., Int. Ed.*, 2015, **54**, 3259–3266.
- 13 F. E. Osterloh, *ACS Energy Lett.*, 2017, **2**, 445–453.
- 14 Y. Tachibana, L. Vayssieres and J. R. Durrant, *Nat. Photonics*, 2012, **6**, 511–518.
- 15 X. Liu, S. Inagaki and J. Gong, *Angew. Chem., Int. Ed.*, 2016, **55**, 14924–14950.
- 16 M. R. Shaner, H. A. Atwater, N. S. Lewis and E. W. McFarland, *Energy Environ. Sci.*, 2016, **9**, 2354–2371.

- 17 C. Xiang, A. Z. Weber, S. Ardo, A. Berger, Y. Chen, R. Coridan, K. T. Fountaine, S. Haussener, S. Hu, R. Liu, N. S. Lewis, M. A. Modestino, M. M. Shaner, M. R. Singh, J. C. Stevens, K. Sun and K. Walczak, *Angew. Chem., Int. Ed.*, 2016, **55**, 12974–12988.
- 18 D. Gust and T. A. Moore, *Science*, 1989, **244**, 35–41.
- 19 R. L. House, N. Y. M. Iha, R. L. Coppo, L. Alibabaei, B. D. Sherman, P. Kang, M. K. Brennaman, P. G. Hoertz and T. J. Meyer, *J. Photochem. Photobiol., C*, 2015, **25**, 32–45.
- 20 W. Kim, E. Edri and H. Frei, *Acc. Chem. Res.*, 2016, **49**, 1634–1645.
- 21 N. S. Lewis, *Nat. Nanotechnol.*, 2016, **11**, 1010–1019.
- 22 D. G. Nocera, *Acc. Chem. Res.*, 2012, **45**, 767–776.
- 23 K. Sivula and R. van de Krol, *Nat. Rev. Mater.*, 2016, **1**, 15010.
- 24 D. Gust, T. A. Moore and A. L. Moore, *Acc. Chem. Res.*, 2001, **34**, 40–48.
- 25 C. W. Cady, R. H. Crabtree and G. W. Brudvig, *Coord. Chem. Rev.*, 2008, **252**, 444–455.
- 26 J. H. Alstrum-Acevedo, M. K. Brennaman and T. J. Meyer, *Inorg. Chem.*, 2005, **44**, 6802–6827.
- 27 I. McConnell, G. Li and G. W. Brudvig, *Chem. Biol.*, 2010, **17**, 434–447.
- 28 L. Sun, L. Hammarstrom, B. Akermark and S. Styring, *Chem. Soc. Rev.*, 2001, **30**, 36–49.
- 29 Y. Chen, S. Hu, C. Xiang and N. S. Lewis, *Energy Environ. Sci.*, 2015, **8**, 876–886.
- 30 H. Inoue, T. Shimada, Y. Kou, Y. Nabetani, D. Masui, S. Takagi and H. Tachibana, *ChemSusChem*, 2011, **4**, 173–179.
- 31 C. C. L. McCrory, S. Jung, I. M. Ferrer, S. M. Chatman, J. C. Peters and T. F. Jaramillo, *J. Am. Chem. Soc.*, 2015, **137**, 4347–4357.
- 32 M. Askerka, G. W. Brudvig and V. S. Batista, *Acc. Chem. Res.*, 2017, **50**, 41–48.
- 33 J. Barber, *Biochemistry*, 2016, **55**, 5901–5906.
- 34 N. Cox, D. A. Pantazis, F. Neese and W. Lubitz, *Acc. Chem. Res.*, 2013, **46**, 1588–1596.
- 35 M. M. Najafpour, S. Heidari, S. E. Balaghi, M. Holynska, M. H. Sadr, B. Soltani, M. Khatamian, A. W. Larkum and S. I. Allakhverdiev, *Biochim. Biophys. Acta, Bioenerg.*, 2017, **1858**, 156–174.
- 36 M. M. Najafpour, G. Renger, M. Holynska, A. N. Moghaddam, E.-M. Aro, R. Carpentier, H. Nishihara, J. J. Eaton-Rye, J.-R. Shen and S. I. Allakhverdiev, *Chem. Rev.*, 2016, **116**, 2886–2936.
- 37 J.-R. Shen, *Annu. Rev. Plant Biol.*, 2015, **66**, 23–48.
- 38 D. J. Vinyard, G. M. Ananyev and G. C. Dismukes, *Annu. Rev. Biochem.*, 2013, **82**, 577–606.
- 39 J. Wang, M. Askerka, G. W. Brudvig and V. S. Batista, *ACS Energy Lett.*, 2017, **2**, 397–407.
- 40 J. Yano and V. Yachandra, *Chem. Rev.*, 2014, **114**, 4175–4205.
- 41 F. Rappaport and B. A. Diner, *Coord. Chem. Rev.*, 2008, **252**, 259–272.
- 42 F. A. Armstrong, *Philos. Trans. R. Soc., B*, 2008, **363**, 1263–1270.
- 43 P. E. M. Siegbahn, *Biochim. Biophys. Acta, Bioenerg.*, 2013, **1827**, 1003–1019.
- 44 J. Messinger, *Phys. Chem. Chem. Phys.*, 2004, **6**, 4764–4771.
- 45 P. E. M. Siegbahn, *Chem. – Eur. J.*, 2006, **12**, 9217–9227.
- 46 H. Dau, C. Limberg, T. Reier, M. Risch, S. Roggan and P. Strasser, *ChemCatChem*, 2010, **2**, 724–761.
- 47 E. M. Sproviero, J. A. Gascon, J. P. McEvoy, G. W. Brudvig and V. S. Batista, *J. Am. Chem. Soc.*, 2008, **130**, 3428–3442.
- 48 J. P. McEvoy and G. W. Brudvig, *Chem. Rev.*, 2006, **106**, 4455–4483.
- 49 T. Taguchi, R. Gupta, B. Lassalle-Kaiser, D. W. Boyce, V. K. Yachandra, W. B. Tolman, J. Yano, M. P. Hendrich and A. S. Borovik, *J. Am. Chem. Soc.*, 2012, **134**, 1996–1999.
- 50 V. L. Pecoraro, M. J. Baldwin, M. T. Caudle, W.-Y. Hsieh and N. A. Law, *Pure Appl. Chem.*, 1998, **70**, 925–929.
- 51 C. Sens, I. Romero, M. Rodriguez, A. Llobet, T. Parella and J. Benet-Buchholz, *J. Am. Chem. Soc.*, 2004, **126**, 7798–7799.
- 52 F. Bozoglian, S. Romain, M. Z. Ertem, T. K. Todorova, C. Sens, J. Mola, M. Rodriguez, I. Romero, J. Benet-Buchholz, X. Fontrodona, C. J. Cramer, L. Gagliardi and A. Llobet, *J. Am. Chem. Soc.*, 2009, **131**, 15176–15187.
- 53 S. Romain, F. Bozoglian, X. Sala and A. Llobet, *J. Am. Chem. Soc.*, 2009, **131**, 2768–2769.
- 54 H. Isobe, K. Tanaka, J.-R. Shen and K. Yamaguchi, *Inorg. Chem.*, 2014, **53**, 3973–3984.
- 55 J. T. Muckerman, D. E. Polyansky, T. Wada, K. Tanaka and E. Fujita, *Inorg. Chem.*, 2008, **47**, 1787–1802.
- 56 T. Wada, H. Ohtsu and K. Tanaka, *Chem. – Eur. J.*, 2012, **18**, 2374–2381.
- 57 T. Wada, K. Tsuge and K. Tanaka, *Angew. Chem., Int. Ed.*, 2000, **39**, 1479–1482.
- 58 T. Wada, K. Tsuge and K. Tanaka, *Inorg. Chem.*, 2001, **40**, 329–337.
- 59 S. Ghosh and M.-H. Baik, *Angew. Chem., Int. Ed.*, 2012, **51**, 1221–1224.
- 60 L. Duan, A. Fischer, Y. Xu and L. Sun, *J. Am. Chem. Soc.*, 2009, **131**, 10397–10399.
- 61 L. Duan, F. Bozoglian, S. Mandal, B. Stewart, T. Privalov, A. Llobet and L. Sun, *Nat. Chem.*, 2012, **4**, 418–423.
- 62 L. Wang, L. Duan, B. Stewart, M. Pu, J. Liu, T. Privalov and L. Sun, *J. Am. Chem. Soc.*, 2012, **134**, 18868–18880.
- 63 J. Nyhlen, L. Duan, B. Akermark, L. Sun and T. Privalov, *Angew. Chem., Int. Ed.*, 2010, **49**, 1773–1777.
- 64 S. W. Gersten, G. J. Samuels and T. J. Meyer, *J. Am. Chem. Soc.*, 1982, **104**, 4029–4030.
- 65 X. Yang and M.-H. Baik, *J. Am. Chem. Soc.*, 2006, **128**, 7476–7485.
- 66 F. Liu, J. J. Concepcion, J. W. Jurss, T. Cardolaccia, J. L. Templeton and T. J. Meyer, *Inorg. Chem.*, 2008, **47**, 1727–1752.
- 67 R. Bianco, P. J. Hay and J. T. Hynes, *J. Phys. Chem. A*, 2011, **115**, 8003–8016.
- 68 A. E. Clark and J. K. Hurst, *Prog. Inorg. Chem.*, John Wiley & Sons, Inc., 2011, vol. 57, pp. 1–54.
- 69 J. J. Concepcion, J. W. Jurss, J. L. Templeton and T. J. Meyer, *J. Am. Chem. Soc.*, 2008, **130**, 16462–16463.

- 70 Z. Chen, J. J. Concepcion, X. Hu, W. Yang, P. G. Hoertz and T. J. Meyer, *Proc. Natl. Acad. Sci. U. S. A.*, 2010, **107**, 7225–7229.
- 71 R. Cao, W. Lai and P. Du, *Energy Environ. Sci.*, 2012, **5**, 8134–8157.
- 72 J. D. Blakemore, R. H. Crabtree and G. W. Brudvig, *Chem. Rev.*, 2015, **115**, 12974–13005.
- 73 A. R. Parent and K. Sakai, *ChemSusChem*, 2014, **7**, 2070–2080.
- 74 R. Brimblecombe, G. C. Dismukes, G. F. Swiegers and L. Spiccia, *Dalton Trans.*, 2009, 9374–9384.
- 75 T. Kikuchi and K. Tanaka, *Eur. J. Inorg. Chem.*, 2014, 607–618.
- 76 X. Sala, S. Maji, R. Bofill, J. Garcia-Anton, L. Escriche and A. Llobet, *Acc. Chem. Res.*, 2014, **47**, 504–516.
- 77 L. Duan, L. Tong, Y. Xu and L. Sun, *Energy Environ. Sci.*, 2011, **4**, 3296–3313.
- 78 D. G. H. Hetterscheid and J. N. H. Reek, *Angew. Chem., Int. Ed.*, 2012, **51**, 9740–9747.
- 79 D. J. Wasylenko, R. D. Palmer and C. P. Berlinguette, *Chem. Commun.*, 2013, **49**, 218–227.
- 80 M. D. Kaerkaes, O. Verho, E. V. Johnston and B. Aakermark, *Chem. Rev.*, 2014, **114**, 11863–12001.
- 81 M. D. Kaerkaes, E. V. Johnston, O. Verho and B. Aakermark, *Acc. Chem. Res.*, 2014, **47**, 100–111.
- 82 M. D. Kaerkaes and B. Aakermark, *Dalton Trans.*, 2016, **45**, 14421–14461.
- 83 G. C. Dismukes, R. Brimblecombe, G. A. N. Felton, R. S. Pryadun, J. E. Sheats, L. Spiccia and G. F. Swiegers, *Acc. Chem. Res.*, 2009, **42**, 1935–1943.
- 84 I. Rivalta, G. W. Brudvig and V. S. Batista, *Molecular Water Oxidation Catalysis*, John Wiley & Sons, Ltd, 2014, pp. 1–14.
- 85 A. Sartorel, M. Bonchio, S. Campagna and F. Scandola, *Chem. Soc. Rev.*, 2013, **42**, 2262–2280.
- 86 T. K. Michaelos, D. Y. Shopov, S. B. Sinha, L. S. Sharninghausen, K. J. Fisher, H. M. C. Lant, R. H. Crabtree and G. W. Brudvig, *Acc. Chem. Res.*, 2017, **50**, 952–959.
- 87 J. J. Concepcion, J. W. Jurss, M. K. Brennaman, P. G. Hoertz, A. O. T. Patrocinio, N. Y. Murakami Iha, J. L. Templeton and T. J. Meyer, *Acc. Chem. Res.*, 2009, **42**, 1954–1965.
- 88 M. Yamamoto and K. Tanaka, *ChemPlusChem*, 2016, **81**, 1028–1044.
- 89 L. Tong and R. P. Thummel, *Chem. Sci.*, 2016, **7**, 6591–6603.
- 90 M. Okamura and S. Masaoka, *Chem. – Asian J.*, 2015, **10**, 306–315.
- 91 F. Puntoriero, A. Sartorel, M. Orlandi, G. La Ganga, S. Serroni, M. Bonchio, F. Scandola and S. Campagna, *Coord. Chem. Rev.*, 2011, **255**, 2594–2601.
- 92 C. J. Gagliardi, A. K. Vannucci, J. J. Concepcion, Z. Chen and T. J. Meyer, *Energy Environ. Sci.*, 2012, **5**, 7704–7717.
- 93 Q. Zeng, F. W. Lewis, L. M. Harwood and F. Hartl, *Coord. Chem. Rev.*, 2015, **304–305**, 88–101.
- 94 A. K. Vannucci, L. Alibabaei, M. D. Losego, J. J. Concepcion, B. Kalanyan, G. N. Parsons and T. J. Meyer, *Proc. Natl. Acad. Sci. U. S. A.*, 2013, **110**, 20918–20922.
- 95 K. J. Young, L. A. Martini, R. L. Milot, R. C. Snoeberger, V. S. Batista, C. A. Schmuttenmaer, R. H. Crabtree and G. W. Brudvig, *Coord. Chem. Rev.*, 2012, **256**, 2503–2520.
- 96 A. R. Parent, R. H. Crabtree and G. W. Brudvig, *Chem. Soc. Rev.*, 2013, **42**, 2247–2252.
- 97 J. J. Stracke and R. G. Finke, *ACS Catal.*, 2014, **4**, 909–933.
- 98 D. W. Shaffer, Y. Xie, D. J. Szalda and J. J. Concepcion, *Inorg. Chem.*, 2016, **55**, 12024–12035.
- 99 S. W. Kohl, L. Weiner, L. Schwartzburd, L. Konstantinovski, L. J. W. Shimon, Y. Ben-David, M. A. Iron and D. Milstein, *Science*, 2009, **324**, 74–77.
- 100 J. P. Collin and J. P. Sauvage, *Inorg. Chem.*, 1986, **25**, 135–141.
- 101 I. Romero, M. Rodríguez, C. Sens, J. Mola, M. Rao Kollipara, L. Francàs, E. Mas-Marza, L. Escriche and A. Llobet, *Inorg. Chem.*, 2008, **47**, 1824–1834.
- 102 R. Zong and R. P. Thummel, *J. Am. Chem. Soc.*, 2005, **127**, 12802–12803.
- 103 P. Huang, A. Magnuson, R. Lomoth, M. Abrahamsson, M. Tamm, L. Sun, B. van Rotterdam, J. Park, L. Hammarström, B. Åkermark and S. Styring, *J. Inorg. Biochem.*, 2002, **91**, 159–172.
- 104 Y. Xu, A. Fischer, L. Duan, L. Tong, E. Gabrielsson, B. Åkermark and L. Sun, *Angew. Chem., Int. Ed.*, 2010, **49**, 8934–8937.
- 105 Y. Jiang, F. Li, B. Zhang, X. Li, X. Wang, F. Huang and L. Sun, *Angew. Chem., Int. Ed.*, 2013, **52**, 3398–3401.
- 106 K. Nagoshi, M. Yagi and M. Kaneko, *Bull. Chem. Soc. Jpn.*, 2000, **73**, 2193–2197.
- 107 F. P. Rotzinger, S. Munavalli, P. Comte, J. K. Hurst, M. Graetzel, F. J. Pern and A. J. Frank, *J. Am. Chem. Soc.*, 1987, **109**, 6619–6626.
- 108 K. Tanaka, H. Isobe, S. Yamanaka and K. Yamaguchi, *Proc. Natl. Acad. Sci. U. S. A.*, 2012, **109**, 15600–15605.
- 109 H. Yamada, W. F. Siems, T. Koike and J. K. Hurst, *J. Am. Chem. Soc.*, 2004, **126**, 9786–9795.
- 110 R. A. Binstead, C. W. Chronister, J. Ni, C. M. Hartshorn and T. J. Meyer, *J. Am. Chem. Soc.*, 2000, **122**, 8464–8473.
- 111 M. M. T. Khan, G. Ramachandraiah, S. H. Mehta, S. H. R. Abdi and S. Kumar, *J. Mol. Catal.*, 1990, **58**, 199–203.
- 112 N. C. Pramanik and S. Bhattacharya, *Transition Met. Chem.*, 1997, **22**, 524–526.
- 113 G. Zhang, R. Zong, H.-W. Tseng and R. P. Thummel, *Inorg. Chem.*, 2008, **47**, 990–998.
- 114 H.-W. Tseng, R. Zong, J. T. Muckerman and R. Thummel, *Inorg. Chem.*, 2008, **47**, 11763–11773.
- 115 Z. Chen, J. J. Concepcion, J. W. Jurss and T. J. Meyer, *J. Am. Chem. Soc.*, 2009, **131**, 15580–15581.
- 116 J. J. Concepcion, M.-K. Tsai, J. T. Muckerman and T. J. Meyer, *J. Am. Chem. Soc.*, 2010, **132**, 1545–1557.
- 117 X. Lin, X. Hu, J. J. Concepcion, Z. Chen, S. Liu, T. J. Meyer and W. Yang, *Proc. Natl. Acad. Sci. U. S. A.*, 2012, **109**, 15669–15672.
- 118 J. J. Concepcion, J. W. Jurss, M. R. Norris, Z. Chen, J. L. Templeton and T. J. Meyer, *Inorg. Chem.*, 2010, **49**, 1277–1279.

- 119 T. J. Meyer, *J. Electrochem. Soc.*, 1984, **131**, 221C–228C.
- 120 A. Dovletoglou, S. A. Adeyemi, M. H. Lynn, D. J. Hodgson and T. J. Meyer, *J. Am. Chem. Soc.*, 1990, **112**, 8989–8990.
- 121 A. Dovletoglou and T. J. Meyer, *J. Am. Chem. Soc.*, 1994, **116**, 215–223.
- 122 T. J. Meyer and M. H. V. Huynh, *Inorg. Chem.*, 2003, **42**, 8140–8160.
- 123 L. Roecker, J. C. Dobson, W. J. Vining and T. J. Meyer, *Inorg. Chem.*, 1987, **26**, 779–781.
- 124 Y. Xie, D. W. Shaffer, A. Lewandowska-Andralojc, D. J. Szalda and J. J. Concepcion, *Angew. Chem., Int. Ed.*, 2016, **55**, 8067–8071.
- 125 J. M. Kamdar, D. C. Marelius, C. E. Moore, A. L. Rheingold, D. K. Smith and D. B. Grotjahn, *ChemCatChem*, 2016, **8**, 3045–3049.
- 126 D. W. Shaffer, Y. Xie, D. J. Szalda and J. J. Concepcion, submitted.
- 127 R. Matheu, M. Z. Ertem, J. Benet-Buchholz, E. Coronado, V. S. Batista, X. Sala and A. Llobet, *J. Am. Chem. Soc.*, 2015, **137**, 10786–10795.
- 128 S. Masaoka and K. Sakai, *Chem. Lett.*, 2009, **38**, 182–183.
- 129 M. Yoshida, S. Masaoka and K. Sakai, *Chem. Lett.*, 2009, **38**, 702–703.
- 130 M. Yoshida, S. Masaoka, J. Abe and K. Sakai, *Chem. – Asian J.*, 2010, **5**, 2369–2378.
- 131 A. Kimoto, K. Yamauchi, M. Yoshida, S. Masaoka and K. Sakai, *Chem. Commun.*, 2012, **48**, 239–241.
- 132 L. Duan, L. Wang, F. Li, F. Li and L. Sun, *Acc. Chem. Res.*, 2015, **48**, 2084–2096.
- 133 L. Wang, L. Duan, Y. Wang, M. S. G. Ahlquist and L. Sun, *Chem. Commun.*, 2014, **50**, 12947–12950.
- 134 L. Duan, L. Wang, A. K. Inge, A. Fischer, X. Zou and L. Sun, *Inorg. Chem.*, 2013, **52**, 7844–7852.
- 135 Y. Xie, D. W. Shaffer, D. J. Szalda and J. J. Concepcion, submitted.
- 136 C. Casadevall, Z. Codolà, M. Costas and J. Lloret-Fillol, *Chem. – Eur. J.*, 2016, **22**, 10111–10126.
- 137 J. L. Fillol, Z. Codolà, I. Garcia-Bosch, L. Gómez, J. J. Pla and M. Costas, *Nat. Chem.*, 2011, **3**, 807–813.
- 138 M. Zhang, M. de Respinis and H. Frei, *Nat. Chem.*, 2014, **6**, 362–367.
- 139 M. Zhang and H. Frei, *Catal. Lett.*, 2015, **145**, 420–435.
- 140 T. Fan, S. Zhan and M. S. G. Ahlquist, *ACS Catal.*, 2016, **6**, 8308–8312.
- 141 T. Ishizuka, H. Kotani and T. Kojima, *Dalton Trans.*, 2016, **45**, 16727–16750.
- 142 N. Planas, L. Vigara, C. Cady, P. Miró, P. Huang, L. Hammarström, S. Styring, N. Leidel, H. Dau, M. Haumann, L. Gagliardi, C. J. Cramer and A. Llobet, *Inorg. Chem.*, 2011, **50**, 11134–11142.
- 143 D. Moonshiram, I. Alperovich, J. J. Concepcion, T. J. Meyer and Y. Pushkar, *Proc. Natl. Acad. Sci. U. S. A.*, 2013, **110**, 3765–3770.
- 144 A. M. Ullman, C. N. Brodsky, N. Li, S.-L. Zheng and D. G. Nocera, *J. Am. Chem. Soc.*, 2016, **138**, 4229–4236.
- 145 S. Koroidov, M. F. Anderlund, S. Styring, A. Thapper and J. Messinger, *Energy Environ. Sci.*, 2015, **8**, 2492–2503.
- 146 S. Maji, L. Vigara, F. Cottone, F. Bozoglian, J. Benet-Buchholz and A. Llobet, *Angew. Chem., Int. Ed.*, 2012, **51**, 5967–5970.
- 147 C. J. Richmond, R. Matheu, A. Poater, L. Falivene, J. Benet-Buchholz, X. Sala, L. Cavallo and A. Llobet, *Chem. – Eur. J.*, 2014, **20**, 17282–17286.
- 148 B. D. Sherman, Y. Xie, M. V. Sheridan, D. Wang, D. W. Shaffer, T. J. Meyer and J. J. Concepcion, *ACS Energy Lett.*, 2017, **2**, 124–128.
- 149 D. W. Crandell, S. Xu, J. M. Smith and M.-H. Baik, *Inorg. Chem.*, 2017, **56**, 4435–4445.
- 150 T. A. Betley, Q. Wu, T. Van Voorhis and D. G. Nocera, *Inorg. Chem.*, 2008, **47**, 1849–1861.
- 151 M. H. V. Huynh and T. J. Meyer, *Chem. Rev.*, 2007, **107**, 5004–5064.
- 152 B. A. Moyer, M. S. Thompson and T. J. Meyer, *J. Am. Chem. Soc.*, 1980, **102**, 2310–2312.
- 153 A. M. Asaduzzaman, D. Wasylenko, C. P. Berlinguette and G. Schreckenbach, *J. Phys. Chem. C*, 2015, **119**, 242–250.
- 154 D. J. Wasylenko, C. Ganesamoorthy, M. A. Henderson, B. D. Koivisto, H. D. Osthoff and C. P. Berlinguette, *J. Am. Chem. Soc.*, 2010, **132**, 16094–16106.
- 155 D. J. Wasylenko, C. Ganesamoorthy, B. D. Koivisto, M. A. Henderson and C. P. Berlinguette, *Inorg. Chem.*, 2010, **49**, 2202–2209.
- 156 K. J. Takeuchi, M. S. Thompson, D. W. Pipes and T. J. Meyer, *Inorg. Chem.*, 1984, **23**, 1845–1851.
- 157 S. A. Trammell, J. C. Wimbish, F. Odobel, L. A. Gallagher, P. M. Narula and T. J. Meyer, *J. Am. Chem. Soc.*, 1998, **120**, 13248–13249.
- 158 M. R. Norris, J. J. Concepcion, D. P. Harrison, R. A. Binstead, D. L. Ashford, Z. Fang, J. L. Templeton and T. J. Meyer, *J. Am. Chem. Soc.*, 2013, **135**, 2080–2083.
- 159 Z. Chen, J. J. Concepcion and T. J. Meyer, *Dalton Trans.*, 2011, **40**, 3789–3792.
- 160 A. Gerli, J. Reedijk, M. T. Lakin and A. L. Spek, *Inorg. Chem.*, 1995, **34**, 1836–1843.
- 161 Z. Chen, A. K. Vannucci, J. J. Concepcion, J. W. Jurss and T. J. Meyer, *Proc. Natl. Acad. Sci. U. S. A.*, 2011, **108**, E1461–E1469.
- 162 C. Costentin, M. Robert and J.-M. Saveant, *Acc. Chem. Res.*, 2010, **43**, 1019–1029.
- 163 E. L. Lebeau, R. A. Binstead and T. J. Meyer, *J. Am. Chem. Soc.*, 2001, **123**, 10535–10544.
- 164 T. J. Meyer, M. H. V. Huynh and H. H. Thorp, *Angew. Chem., Int. Ed.*, 2007, **46**, 5284–5304.
- 165 J. J. Concepcion, R. A. Binstead, L. Alibabaei and T. J. Meyer, *Inorg. Chem.*, 2013, **52**, 10744–10746.
- 166 B. T. Farrer and H. H. Thorp, *Inorg. Chem.*, 1999, **38**, 2497–2502.
- 167 J. T. Muckerman, M. Kowalczyk, Y. M. Badiei, D. E. Polyansky, J. J. Concepcion, R. Zong, R. P. Thummel and E. Fujita, *Inorg. Chem.*, 2014, **53**, 6904–6913.
- 168 R. Zong and R. P. Thummel, *J. Am. Chem. Soc.*, 2004, **126**, 10800–10801.
- 169 Y. Liu, S.-M. Ng, S.-M. Yiu, W. W. Y. Lam, X.-G. Wei, K.-C. Lau and T.-C. Lau, *Angew. Chem., Int. Ed.*, 2014, **53**, 14468–14471.

- 170 J. J. Concepcion, D. K. Zhong, D. J. Szalda, J. T. Muckerman and E. Fujita, *Chem. Commun.*, 2015, **51**, 4105–4108.
- 171 N. Song, J. J. Concepcion, R. A. Binstead, J. A. Rudd, A. K. Vannucci, C. J. Dares, M. K. Coggins and T. J. Meyer, *Proc. Natl. Acad. Sci. U. S. A.*, 2015, **112**, 4935–4940.
- 172 Q. Daniel, P. Huang, T. Fan, Y. Wang, L. Duan, L. Wang, F. Li, Z. Rinkevicius, F. Mamedov, M. S. G. Ahlquist, S. Styring and L. Sun, *Coord. Chem. Rev.*, 2017, **346**, 206–215.
- 173 X. Yang and M.-H. Baik, *J. Am. Chem. Soc.*, 2008, **130**, 16231–16240.
- 174 M. V. Sheridan, B. D. Sherman, S. L. Marquard, Z. Fang, D. L. Ashford, K.-R. Wee, A. S. Gold, L. Alibabaei, J. A. Rudd, M. K. Coggins and T. J. Meyer, *J. Phys. Chem. C*, 2015, **119**, 25420–25428.
- 175 M. Schulze, V. Kunz, P. D. Frischmann and F. Würthner, *Nat. Chem.*, 2016, **8**, 576–583.
- 176 Y. Sato, S.-y. Takizawa and S. Murata, *Eur. J. Inorg. Chem.*, 2015, 5495–5502.
- 177 E. M. Duffy, B. M. Marsh, J. M. Voss and E. Garand, *Angew. Chem., Int. Ed.*, 2016, **55**, 4079–4082.
- 178 M. V. Sheridan, B. D. Sherman, Z. Fang, K.-R. Wee, M. K. Coggins and T. J. Meyer, *ACS Catal.*, 2015, **5**, 4404–4409.
- 179 S. Neudeck, S. Maji, I. López, S. Meyer, F. Meyer and A. Llobet, *J. Am. Chem. Soc.*, 2014, **136**, 24–27.
- 180 A. C. Sander, S. Maji, L. Francàs, T. Böhnisch, S. Dechert, A. Llobet and F. Meyer, *ChemSusChem*, 2015, **8**, 1697–1702.
- 181 L. L. Zhang, Y. Gao, Z. Liu, X. Ding, Z. Yu and L. C. Sun, *Dalton Trans.*, 2016, **45**, 3814–3819.
- 182 D. L. Ashford, B. D. Sherman, R. A. Binstead, J. L. Templeton and T. J. Meyer, *Angew. Chem., Int. Ed.*, 2015, **54**, 4778–4781.
- 183 Y. Gao, X. Ding, J. Liu, L. Wang, Z. Lu, L. Li and L. Sun, *J. Am. Chem. Soc.*, 2013, **135**, 4219–4222.
- 184 F. Li, K. Fan, L. Wang, Q. Daniel, L. Duan and L. Sun, *ACS Catal.*, 2015, **5**, 3786–3790.
- 185 M. V. Sheridan, B. D. Sherman, R. L. Coppo, D. Wang, S. L. Marquard, K.-R. Wee, N. Y. Murakamiha and T. J. Meyer, *ACS Energy Lett.*, 2016, **1**, 231–236.
- 186 B. D. Sherman, D. L. Ashford, A. M. Lapides, M. V. Sheridan, K.-R. Wee and T. J. Meyer, *J. Phys. Chem. Lett.*, 2015, **6**, 3213–3217.
- 187 B. D. Sherman, M. V. Sheridan, K.-R. Wee, S. L. Marquard, D. Wang, L. Alibabaei, D. L. Ashford and T. J. Meyer, *J. Am. Chem. Soc.*, 2016, **138**, 16745–16753.
- 188 L. Wang, K. Fan, H. Chen, Q. Daniel, B. Philippe, H. Rensmo and L. Sun, *Catal. Today*, 2017, **290**, 73–77.
- 189 L. Wang, M. Mirmohades, A. Brown, L. Duan, F. Li, Q. Daniel, R. Lomoth, L. Sun and L. Hammarstroem, *Inorg. Chem.*, 2015, **54**, 2742–2751.
- 190 J. Mola, E. Mas-Marza, X. Sala, I. Romero, M. Rodriguez, C. Vinas, T. Parella and A. Llobet, *Angew. Chem., Int. Ed.*, 2008, **47**, 5830–5832.
- 191 L. Alibabaei, M. K. Brennaman, M. R. Norris, B. Kalanyan, W. Song, M. D. Losego, J. J. Concepcion, R. A. Binstead, G. N. Parsons and T. J. Meyer, *Proc. Natl. Acad. Sci. U. S. A.*, 2013, **110**, 20008–20013.
- 192 D. L. Ashford, W. Song, J. J. Concepcion, C. R. K. Glasson, M. K. Brennaman, M. R. Norris, Z. Fang, J. L. Templeton and T. J. Meyer, *J. Am. Chem. Soc.*, 2012, **134**, 19189–19198.
- 193 S. E. Bettis, K. Hanson, L. Wang, M. K. Gish, J. J. Concepcion, Z. Fang, T. J. Meyer and J. M. Papanikolas, *J. Phys. Chem. A*, 2014, **118**, 10301–10308.
- 194 J. J. Concepcion, J. W. Jurss, P. G. Hoertz and T. J. Meyer, *Angew. Chem., Int. Ed.*, 2009, **48**, 9473–9476.
- 195 C. R. K. Glasson, W. Song, D. L. Ashford, A. Vannucci, Z. Chen, J. J. Concepcion, P. L. Holland and T. J. Meyer, *Inorg. Chem.*, 2012, **51**, 8637–8639.
- 196 K. Hanson, D. A. Torelli, A. K. Vannucci, M. K. Brennaman, H. Luo, L. Alibabaei, W. Song, D. L. Ashford, M. R. Norris, C. R. K. Glasson, J. J. Concepcion and T. J. Meyer, *Angew. Chem., Int. Ed.*, 2012, **51**, 12782–12785.
- 197 A. Nayak, R. R. Knauf, K. Hanson, L. Alibabaei, J. J. Concepcion, D. L. Ashford, J. L. Dempsey and T. J. Meyer, *Chem. Sci.*, 2014, **5**, 3115–3119.
- 198 M. R. Norris, J. J. Concepcion, Z. Fang, J. L. Templeton and T. J. Meyer, *Angew. Chem., Int. Ed.*, 2013, **52**, 13580–13583.
- 199 W. Song, C. R. K. Glasson, H. Luo, K. Hanson, M. K. Brennaman, J. J. Concepcion and T. J. Meyer, *J. Phys. Chem. Lett.*, 2011, **2**, 1808–1813.
- 200 D. J. Stewart, J. J. Concepcion, M. K. Brennaman, R. A. Binstead and T. J. Meyer, *Proc. Natl. Acad. Sci. U. S. A.*, 2013, **110**, 876–880.